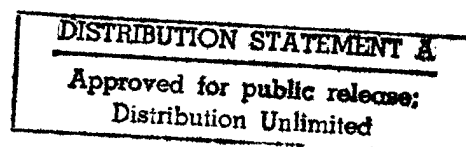Inverse Scattering via Heisenberg's Uncertainty Principle

Yu Chen
Research Report YALEU/DCS/RR-1091
February 1996

19960313 060

DTIC QUALITY INSPECTED 1

YALE UNIVERSITY
DEPARTMENT OF COMPUTER SCIENCE

We present a stable method to recursively linearize the acoustic inverse scattering problem. It turns out that the ill-posedness of the problem can be beneficially used to solve it. It means that, due to ill-posedness, not all equations in the nonlinear system are strongly nonlinear, and that when solved recursively in a proper order, they can be reduced to a collection of linear problems.

Our method requires solution of a series of forward scattering problems with ascending wave numbers (or frequencies). At each frequency, a linear least-squares problem is solved to obtain an approximate forward model which produces the prescribed scattering data. The robustness of the procedure is demonstrated by several numerical examples in the inversion of the Helmholtz equation in two dimensions.

Inverse Scattering via Heisenberg's Uncertainty Principle

Yu Chen
Research Report YALEU/DCS/RR-1091
February 1996

1   Introduction

The solution of the inverse scattering problem requires, in essence, an inversion of a nonlinear mapping. There are two major difficulties associated with this nonlinear problem in two and three dimensions : ill-posedness and local minima, neither of which has been addressed satisfactorily. The fact alone that the nonlinear system at high wave number is extremely oscillatory and therefore possesses numerous local minima renders the most popular approach—nonlinear optimization and its various modifications—fundamentally unreliable. In another notable approach to attacking the nonlinear problem, the original boundary value problem is reformulated as an initial value problem. The resulting method (known under several names such as layer-stripping, trace method) avoids the problem of local minima, only to be plagued by ill-posedness. There are still other approaches which compromise in some way but have not yet been able to squeeze through the flails of these two perils.

We present a stable method that solves the inverse scattering problem. It turns out that the ill-posedness of the inverse problem can be beneficially used to solve it. It means that not all equations in the nonlinear system are strongly nonlinear, and that when solved recursively in a proper order, they can be reduced to a collection of linear problems.

Our method requires solutions of a series of forward scattering problems with ascending wave numbers (or frequencies). At each frequency, a linear least-squares problem is solved to obtain an approximate index of refraction which not only minimizes, but also eliminates the discrepancy between the prescribed and the predicted scattering data. The robustness of the procedure is illustrated by several numerical examples in the inversion of the Helmholtz equation in two dimensions.

The plan of the paper is as follows: in Section 2 we summerize the relevant analytical apparatus, in Section 3 we reformulate the ill-posedness and the inverse scattering problem, and present the inversion method, and in Section 4 we describe the numerical implementation of the algorithm. The robustness of the procedure is demonstrated with numerical examples in Section 5.

2   The Mathematical Preliminaries

In this section we summarize several analytical results regarding the scattering problem, the solution of a nonlinear problem, and the solution of linear ordinary differential equations of matrices.

1

2.1 The Scattering Problem

The subject of this paper is the inverse scattering problem for Helmholtz equation in two dimensions

$$\Delta\phi(x,y) + k^2(1 + q(x,y))\phi(x,y) = 0. \tag{1}$$

In (1), k is a real number, q a smooth function, with $q(x) > -1$ for all $x \in R^2$. We will be referring to k as the wave number or frequency, to the function q as the scatterer or the forward model. We assume that the support of q is a disk $D(\varpi)$ defined by the formula

$$D(\varpi) = \{ (x,y) \mid x^2 + y^2 \le \varpi^2 \} \tag{2}$$

for some $\varpi > 0$. We will be considering solutions of equation (1) of the form

$$\phi(x,y) = \phi_0(x,y) + \psi(x,y), \tag{3}$$

with $\phi_0 : D(\varpi) \to C$ a solution of the equation

$$\Delta\phi_0(x,y) + k^2\phi_0(x,y) = 0 \tag{4}$$

(to which we will be referring as the homogeneous Helmholtz equation), and $\psi : R^2 \to C$ the solution of the equation

$$\Delta\psi(x,y) + k^2(1 + q(x,y))\psi(x,y) = -k^2 q(x,y)\phi_0(x,y), \tag{5}$$

subject to the outgoing (Sommerfeld) radiation condition

$$\lim_{r\to\infty} \sqrt{r}\left(\frac{\partial\psi}{\partial r} - ik\psi\right) = 0. \tag{6}$$

We will be referring to ϕ as the total field, to ϕ_0 as the incident field, and to ψ as the scattered field. Furthermore, given an incident field ϕ_0 we will be referring to the determination of the corresponding scattered field as the (forward) scattering problem.

Remark 2.1 *We measure the size of the scatterer by the number of wavelengths through the longest ray tube. More precisely, suppose that the curve $\ell \subset D(\varpi)$ is the longest ray tube, and ds is the arc length element on ℓ; then the number of wavelengths across ℓ is given by the formula is*

$$N_w = \frac{k}{2\pi}\int_\ell \sqrt{1 + q(x,y)}ds. \tag{7}$$

When the medium is quite homogeneous, namely, when q is small, and thus the ray path is roughly straight, (7) is reduced to

$$N_w = \frac{k\cdot\varpi}{\pi}. \tag{8}$$

2

2.2 The Scattering Matrix and Scattering Data

In this subsection, we reformulate the scattering problem introduced in the preceding subsection via the scattering matrix. For a more complete description and analysis of the scattering matrix, see [11]. Denote by J_m the Bessel function of the first kind of order m, by Y_m the Neumann function (or the Bessel function of the second kind) of order m, and by H_m Hankel function of the first kind of order m, so that

$$H_m = J_m + i \cdot Y_m. \tag{9}$$

Given a positive number z, we will denote by X_z the linear space of all two-sided complex sequences $\{\alpha_m\}$ such that for some $c > 0$

$$|\alpha_m \cdot J_m(z)| < c, \tag{10}$$

for all integer m. We will denote by Y_z the linear space of all two-sided complex sequences $\{\beta_m\}$ such that for some $c > 0$

$$|\beta_m \cdot H_m(z)| < c, \tag{11}$$

for all integer m.

Remark 2.2 *It is well-known (see, for example, [4], [5], [3]) that once the positive number ν is greater than z, the Bessel function $J_\nu(z)$ strictly decays as ν grows, and that the Neumann function $Y_\nu(z)$ strictly grows as ν grows. Moreover, $J_\nu(z)$ becomes very small, and $Y_\nu(z)$ becomes very large, when ν reaches*

$$N_0(z) = z + O\left(z^{\frac{1}{3}}\right). \tag{12}$$

Finally, for $\nu \geq N_0(z)$,

$$J_m(z) \sim \frac{1}{\sqrt{2\pi m}} \cdot \left(\frac{e \cdot z}{2m}\right)^m, \tag{13}$$

$$H_m(z) \sim -i \cdot \sqrt{\frac{2}{\pi m}} \cdot \left(\frac{2m}{e \cdot z}\right)^m. \tag{14}$$

Remark 2.3 *Formulae (10) and (11) can be rewritten as*

$$|\alpha_m| \cdot \left(\frac{e \cdot z}{2|m|}\right)^{|m|} \cdot \sqrt{|m|} < c, \tag{15}$$

$$|\beta_m| \cdot \left(\frac{2|m|}{e \cdot z}\right)^{|m|} \cdot \sqrt{|m|} < c. \tag{16}$$

3

It is well-known (see, for example, [1], [11] for details) that inside disk $D(\varpi)$, the solution ϕ_0 of the homogeneous Helmholtz equation (4) can be expressed as

$$\phi_0(r,\theta) = \sum_{m=-\infty}^{\infty} \alpha_m \cdot J_m(kr) \cdot e^{im\theta}, \tag{17}$$

with the sequence $\alpha = \{\alpha_m\} \in X_{k\varpi}$, and that outside $D(\varpi)$, the scattered field ψ can be expressed as

$$\psi(r,\theta) = \sum_{m=-\infty}^{\infty} \beta_m \cdot H_m(kr) \cdot e^{im\theta}. \tag{18}$$

with the sequence $\beta = \{\beta_m\} \in Y_{k\varpi}$. The well-posedness of the scattering problem implies a linear mapping $S_{\varpi,k} : X_{k\varpi} \mapsto Y_{k\varpi}$ defined by the formula

$$\beta = S_{\varpi,k} \cdot \alpha, \tag{19}$$

for every $\alpha = \{\alpha_m\} \in X_{k\varpi}$ of the incident field (17) and $\beta = \{\beta_m\} \in Y_{k\varpi}$ of the corresponding scattered field (18). The linear mapping $S_{\varpi,k}$ is refered to as the scattering matrix corresponding to the scatterer q in $D(\varpi)$. For a fixed $k > 0$, the scattering matrix is evidently all we can acquire from scattering measurements outside the disk $D(\varpi)$. The set of matrices

$$\{\, S_{\varpi,k} \mid 0 < k < \infty \,\} \tag{20}$$

is all the information we can collect from real-frequency measurements, and is defined as our scattering data.

Definition 2.4 *An aperture (of acoustic measurement) is an area in the square $[0,2\pi] \times [0,2\pi]$; the full aperture is the entire square. A Fourier aperture is an area in the (two-dimensional) Fourier space, and for such an area E, a function $g \in L^2(\Omega)$ is said to be specified on a Fourier aperture E if its Fourier transform $\hat{g}_{m,n}$ is known for all points $(m,n) \in E$.*

Remark 2.5 *The knowledge of the scattering matrix $S_{\varpi,k}$ is equivalent to that of the full-aperture measurements taken outside $D(\varpi)$, that is, the acquisition of each scattered field ψ outside $D(\varpi)$ corresponding to every possible incident field ϕ_0; see (56), (57) for further details.*

Remark 2.6 *Obviously, for a given positive number r, the above analysis and definition can be applied to a scatterer located on the disk $D(r)$. In particular, there is a scattering matrix, denoted by $S_{r,k}$, corresponding to this disk scatterer.*

Remark 2.7 *For two positive numbers $r_1 < r_2$, a scatterer in the disk $D(r_1)$ can always be regarded as a scatterer in the larger disk $D(r_2)$. Therefore, there are two scattering matrices, $S_{r_1,k}$ and $S_{r_2,k}$, corresponding to the same scatterer on the two concentric disks. It is easy to verify that the two matrices are identical.*

4

2.3 The Riccati Matrix Equation

We show in this subsection that the scattering matrix $S_{\varpi,k}$ is a member of a family of scattering matrices governed by a Riccati equation. For a more complete discussion of the Riccati matrix equation, see [11]. For $r > 0$, following the standard procedure of invariant embedding, we define the chopped scatterer $q_{D(r)}$ by the formula

$$q_{D(r)}(\rho,\theta) = \begin{cases} q(\rho,\theta) & \text{if } \rho < r, \\ 0 & \text{if } \rho \geq r. \end{cases} \tag{21}$$

We will denote by $S_{r,k} : X_{kr} \mapsto Y_{kr}$ the scattering matrix (see Remark 2.6) corresponding to the chopped scatterer. In other words, for every $\alpha \in X_{kr}$ there exists $\beta \in Y_{kr}$ such that

$$\beta = S_{r,k} \cdot \alpha \tag{22}$$

where

$$\psi(\rho,\theta) = \sum_{m=-\infty}^{\infty} \beta_m \cdot H_m(k\rho) \cdot e^{im\theta} \tag{23}$$

is the scattered field outside $D(r)$ corresponding to the incident field

$$\phi_0(\rho,\theta) = \sum_{m=-\infty}^{\infty} \alpha_m \cdot J_m(k\rho) \cdot e^{im\theta} \tag{24}$$

upon the scatterer $q_{D(r)}$. For any $r \geq \varpi$,

$$S_{r,k} = S_{\varpi,k}, \tag{25}$$

due to Remark 2.7. At $r = 0$, the chopped scatterer $q_{D(r)}$ is identically zero; any incident field generates no scattered field. Thus,

$$S_{0,k} = 0. \tag{26}$$

Now we need the following notation in order to present a ordinary differential equation for $S_{r,k}$. Denote by J_z, H_z the diagonal matrices

$$J_z = diag\{\ldots, J_{-1}(z), J_0(z), J_1(z), \ldots\}, \tag{27}$$
$$H_z = diag\{\ldots, H_{-1}(z), H_0(z), H_1(z), \ldots\}, \tag{28}$$

and by F the Fourier transform converting a function in $L^2[0, 2\pi]$ to its Fourier coefficients in ℓ^2. Let

$$\hat{g}_m(r) = \frac{1}{2\pi} \int_0^{2\pi} g(r,\theta) e^{im\theta} d\theta, \tag{29}$$

for a smooth function $g : R^2 \mapsto C$, and let $\hat{g}_r$ be the matrix whose (m,n)-th entry is defined by the formula

$$(\hat{g}_r)_{m,n} = \hat{g}_{m-n}(r). \tag{30}$$

5

Remark 2.8 *Denoting by* $g_r : L^2[0, 2\pi] \mapsto L^2[0, 2\pi]$ *the diagonal linear mapping*

$$(g_r \cdot f)(\theta) = g(r, \theta) \cdot f(\theta) \tag{31}$$

for all $f \in L^2[0, 2\pi]$, *we can easily verify that*

$$\hat{g}_r = F \cdot g_r \cdot F^{-1}. \tag{32}$$

Obviously, for the scatterer function q, $\hat{q}_r$ is a Toeplitz matrix whose first quadrant (entries with both row and column indices positive) is of the form

$$
\hat{q}_r = \begin{bmatrix}
\hat{q}_0(r) & \hat{q}_{-1}(r) & \hat{q}_{-2}(r) & \hat{q}_{-3}(r) & \hat{q}_{-4}(r) & \hat{q}_{-5}(r) & \cdots \\
\hat{q}_1(r) & \hat{q}_0(r) & \hat{q}_{-1}(r) & \hat{q}_{-2}(r) & \hat{q}_{-3}(r) & \hat{q}_{-4}(r) & \cdots \\
\hat{q}_2(r) & \hat{q}_1(r) & \hat{q}_0(r) & \hat{q}_{-1}(r) & \hat{q}_{-2}(r) & \hat{q}_{-3}(r) & \cdots \\
\hat{q}_3(r) & \hat{q}_2(r) & \hat{q}_1(r) & \hat{q}_0(r) & \hat{q}_{-1}(r) & \hat{q}_{-2}(r) & \cdots \\
\hat{q}_4(r) & \hat{q}_3(r) & \hat{q}_2(r) & \hat{q}_1(r) & \hat{q}_0(r) & \hat{q}_{-1}(r) & \cdots \\
\hat{q}_5(r) & \hat{q}_4(r) & \hat{q}_3(r) & \hat{q}_2(r) & \hat{q}_1(r) & \hat{q}_0(r) & \cdots \\
& \cdot & \cdot & \cdot & \cdot & \cdot & \cdots
\end{bmatrix}. \tag{33}
$$

As a function of r, the scattering matrix $S_{r,k}$ satisfies a Riccati equation, see [11] for details.

Lemma 2.9 *For any $k > 0$ and all $r \geq 0$, the scattering matrix $S_{r,k} : X_{kr} \mapsto Y_{kr}$ is a solution of the Riccati equation*

$$\frac{dS_{r,k}}{dr} = \frac{i\pi r}{2} k^2 (J_{kr} + S_{r,k} \cdot H_{kr}) \cdot \hat{q}_r \cdot (H_{kr} \cdot S_{r,k} + J_{kr}). \tag{34}$$

In the reminder of this paper, we assume that the initial value problem defined by (34) and (26) is well-posed, and that the entries of the matrix $S_{r,k}$ depend on (r, k) smoothly.

Remark 2.10 *Given k and q, the initial value problem of the Riccati equation (see (34) and (26)) will be solved in the forward modeling of the inversion algorithm described in Section 3.6; see (146), (147) for details.*

Remark 2.11 *According to formulae (10) and (11), the sequence $\alpha = \{\alpha_m\}$ in (22) may grow as fast as $J_m^{-1}(kr)$, whereas the sequence $\beta = \{\beta_m\}$ in (22) must decay at least as fast as $H_m^{-1}(kr)$. Therefore, Remark 2.2 and the fact*

$$\beta_m = (S_{r,k})_{m,n} \cdot \alpha_n \tag{35}$$

6

implies that

$$(S_{r,k})_{m,n} \;=\; O\left(H_m^{-1}(kr)\right), \tag{36}$$

$$(S_{r,k})_{n,m} \;=\; O\left(J_m(kr)\right), \tag{37}$$

for an arbitrary integer n and large integer $m \geq N_0(kr)$. Thus, the entries of $S_{r,k}$ whose row or column indices are greater in absolute value than $N_0(kr)$ are essentially zero (see Figure 1); the dimension of scattering matrix $S_{r,k}$ is effectually finite: it is essentially a square matrix of dimension $2 \cdot N_0(kr)$.

The structure of the first quadrant (entries with both row and column indices positive) of the matrix $S_{r,k}$ is shown in Figure 1. In the figure, a part of a matrix is labeled zero to indicate that the entries in that part of the matrix are essentially zero.
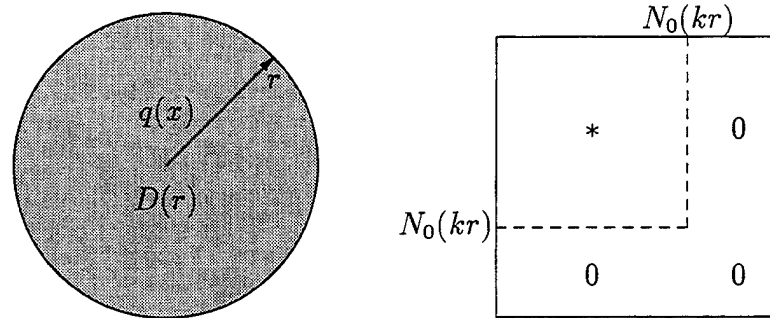

Figure 1: Scatterer on $D(r)$ and Structure of Its Scattering Matrix $S_{r,k}$.

Remark 2.12 *Given an operator $\mathcal{F}$ which maps from one linear space X to another Y, we will casually use the term* virtually-null *space of $\mathcal{F}$: an element $\xi \in X$ belongs to the virtually-null space if $\mathcal{F}(\xi)$ is small. We will also loosely use the phrase* virtual rank *of an operator in accordance with the term* virtually-null *space; the virtual rank of the scattering matrix $S_{r,k}$, for instance, is no greater than $2 \cdot N_0(r,k)$ (see Remark 2.11). We may further think of virtual rank as a real number.*

Remark 2.13 *Given positive numbers k and r, according to Remark 2.2, the diagonal matrix J_{kr} is essentially a square matrix of dimension $2 \cdot N_0(kr)$. Therefore, up to $O[(kr)^{\frac{1}{3}}]$, the matrix J_{kr} can be regarded as to have the same structure as that of $S_{r,k}$ (see Figure 1).*

Remark 2.14 *Given positive numbers k and r, combining (35) with formulae (10), (11), we obtain*

$$(S_{r,k} \cdot H_{kr})_{n,m} \;=\; O\left(H_m^{-1}(kr)\right), \tag{38}$$

$$(H_{kr} \cdot S_{r,k})_{m,n} \;=\; O\left(J_m(kr)\right), \tag{39}$$

7

for an arbitrary integer m and large integers $n \geq N_0(kr)$. In other words, the matrix $S_{r,k} \cdot H_{kr}$ only has $2 \cdot N_0(kr)$ effectually nonzero rows—the rest of the rows whose indices are greater in absolute value than $N_0(kr)$ are essentially zero. Similarly, the number of effectually nonzero columns of $H_{kr} \cdot S_{r,k}$ is also $2 \cdot N_0(kr)$.

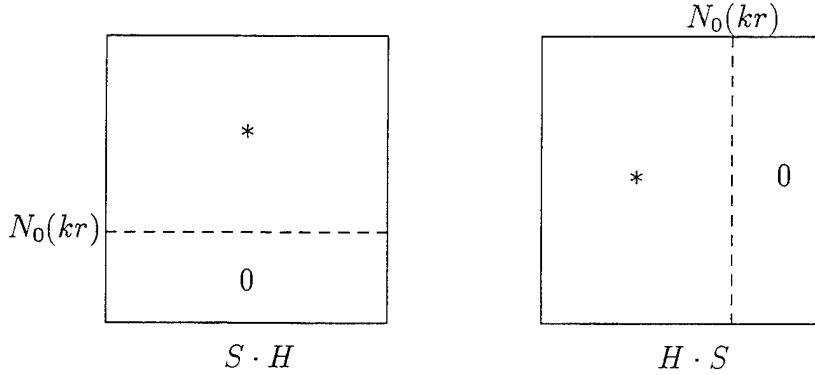Figure 2: Structures of the Matrices $S_{r,k} \cdot H_{kr}$, $H_{kr} \cdot S_{r,k}$.

Figure 2 shows the structures of the two matrices $S_{r,k} \cdot H_{kr}$ and $H_{kr} \cdot S_{r,k}$. Only the first quadrant of the matrices (entries with both row and column indices positive) is depicted here. In the figure, a section of a matrix is labeled zero to indicate that the entries in that part of the matrix are essentially zero.

Remark 2.15 *Given a frequency $k > 0$, the forward scattering problem (see Section 2.1 and Remark 2.10) defines a nonlinear mapping from the scatterer q on $D(\varpi)$ to the scattering data $S_{\varpi,k}$. The initial value problem defined by (34) and (26) turns out to be a convenient tool for analyzing and numerically treating this nonlinear system. According to Remark 2.11, $S_{\varpi,k}$ only has $(2 \cdot N_0(k\varpi))^2$ entries essentially nonzero; therefore, there will be the same number of equations in the nonlinear system.*

Finally in this subsection, we show some basic algebraic properties of the matrix Riccati equation and the scattering matrix.

Definition 2.16 *Suppose that N is a positive integer or $+\infty$. For a square matrix $A = (a_{i,j}, -N < i, j < N)$ of dimension $2N - 1$, define*

$$B = A^\tau = (b_{i,j}, -N < i, j < N), \tag{40}$$
$$b_{i,j} = (-1)^{i+j} \cdot a_{-j,-i}. \tag{41}$$

Clearly, the operator $(\cdots)^\tau$ defines a linear mapping from $C^{(2N-1) \times (2N-1)}$ to itself. The following lemma is a direct consequence of Definition 2.16.

Lemma 2.17 *Suppose that N is a positive integer or $+\infty$. Suppose further that A, B are two matrices and I is the identity matrix in $C^{(2N-1)\times(2N-1)}$. Finally, suppose that $\Upsilon \in C^{(2N-1)\times(2N-1)}$ is the diagonal matrix $\Upsilon_{i,i} = (-1)^i$. Then*

$$(A \cdot B)^\tau = B^\tau \cdot A^\tau, \tag{42}$$

$$(A^\tau)^\tau = A, \tag{43}$$

$$I^\tau = I, \tag{44}$$

$$\Upsilon^\tau = \Upsilon. \tag{45}$$

The following lemma is a direct consequence of Lemmas 2.17 and 2.9.

Lemma 2.18 *Suppose that r, k are positive numbers, and that $S_{r,k}$ is the scattering matrix corresponding to the chopped scatterer $q_{D(r)}$. Suppose further that Υ is diagonal matrix of infinite dimension defined by $\Upsilon_{i,i} = (-1)^i$. Then*

$$(J_{kr})^\tau = \Upsilon \cdot J_{kr} = J_{kr} \cdot \Upsilon, \tag{46}$$

$$(H_{kr})^\tau = \Upsilon \cdot H_{kr} = H_{kr} \cdot \Upsilon, \tag{47}$$

$$(\hat{q}_r)^\tau = \Upsilon \cdot \hat{q}_r \cdot \Upsilon, \tag{48}$$

$$(S_{r,k})^\tau = S_{r,k}. \tag{49}$$

2.4 The Far Field

In this subsection, we first define the far field of a scattered field, and link it to the scattering matrix. We then introduce the translation operator of the scattering matrix. We will require the column-vector F_θ and the row-vector F_θ^{-1} defined by

$$F_\theta = \{ e^{-im\theta}, m = \ldots, -2, -1, 0, 1, 2, \ldots \}^T, \tag{50}$$

$$F_\theta^{-1} = \{ e^{im\theta}, m = \ldots, -2, -1, 0, 1, 2, \ldots \}, \tag{51}$$

and the diagonal matrix Λ defined by

$$\Lambda = diag\{\ldots, i^{-2}, i^{-1}, 1, i, i^2, \ldots\}. \tag{52}$$

Lemma 2.19 *Given $k > 0$, there exists a function $\psi_\infty : [0, 2\pi] \mapsto C$, such that for large $r > 0$, the scattered field (18) assumes the form*

$$\psi(r, \theta) = \sqrt{\frac{2}{\pi kr}} e^{i(kr - \pi/4)} \cdot \left(\psi_\infty(\theta) + O\left(\frac{1}{kr}\right) \right). \tag{53}$$

Proof. For arbitrary integer m and large $z > |m|$ (see [3], pp 364),

$$H_m(z) = \sqrt{\frac{2}{\pi z}} e^{i(z - \pi/4)} \cdot \left(i^{-m} + O\left(\frac{1}{z}\right) \right). \tag{54}$$

The lemma follows immediately from the combination of (54) and (18). □

9

Definition 2.20 *Suppose that ψ is a scattered field; then the function*

$$\psi_\infty(\theta) = \lim_{r \to \infty} \frac{\psi(r, \theta)}{\sqrt{\frac{2}{\pi k r}} e^{i(kr - \pi/4)}} \tag{55}$$

is referred to as the far field of ψ.

Given the incident angle $\beta \in [0, 2\pi]$ and the incident field

$$\phi_0(x, y) = e^{ik(x \cos \beta + y \sin \beta)} = e^{ikr \cos(\theta - \beta)}, \tag{56}$$

we denote by $\psi(r, \theta; \beta)$ the corresponding scattered field, and by

$$\psi_\infty(\theta, \beta) = \frac{\psi(r, \theta; \beta)}{\sqrt{\frac{2}{\pi k r}} e^{i(kr - \pi/4)}} \tag{57}$$

the far field of the scattered field $\psi(r, \theta; \beta)$. The function (57) is frequently referred to as the (far-field, full-aperture) scattering amplitude (see, for example, [2] and [6]). The full-aperture scattering amplitude is related to the scattering matrix (see Remark 2.5) via orthogonal transforms specified in the following lemma.

Lemma 2.21 *Suppose that b is a positive number and S is the scattering matrix corresponding to a scatterer in the disk $D(b)$. Suppose further that $\psi_\infty(\theta, \beta)$ is the scattering amplitude. Then*

$$\psi_\infty(\theta, \beta) = \sum_{m,l} i^{(l-m)} \cdot S_{m,l} \cdot e^{i(m\theta - l\beta)}, \tag{58}$$

or equivalently,

$$\psi_\infty(\theta, \beta) = F_\theta^{-1} \cdot \Lambda^{-1} \cdot S \cdot \Lambda \cdot F_\beta. \tag{59}$$

Proof. It is easy to verify that the incident field (56) can be written in the form (17) with

$$\alpha = \Lambda \cdot F(\beta). \tag{60}$$

The corresponding scattered field (18) therefore is

$$\psi(r, \theta; \beta) = F_\theta^{-1} \cdot H_{kr} \cdot \gamma, \tag{61}$$

with

$$\gamma = S \cdot \alpha. \tag{62}$$

Substituting (60) into (62) which is in turn substituted into (61), we obtain

$$\psi(r, \theta; \beta) = F_\theta^{-1} \cdot H_{kr} \cdot S \cdot \Lambda \cdot F_\beta. \tag{63}$$

10

Now the lemma follows immediately from the combination of (63), (57) and (54).
□

We say that the scattering matrix $S_{\varpi,k}$ corresponding to the scatterer q is centered at the origin $(0,0)$ since the expansions (17) and (18) of the incident and scattered fields are around the origin. Now, for the same physical scatterer, if we shift the origin to a point $\xi = (a,b)$, the new scatterer function will be $q^\xi(x,y) = q(x-a, y-b)$ in the new coordinates. It has compact support in the disk $D(A)$, $A = \varpi + |\xi|$, centered at the new origin. We denote by $S^\xi_{A,k}$ the scattering matrix, corresponding to the same scatterer, but centered at ξ. The following lemma is a reformulation of Lemmas 3.2, 3.3 of [7].

Lemma 2.22 *Suppose that q is the function of a smooth scatterer with compact support $D(\varpi)$, that $u = (x_1, y_1)$, $v = (x_2, y_2)$ are two points in R^2, and that $A = \varpi + |u|$, $B = \varpi + |v|$. Suppose further that, corresponding to the same scatterer, $S^u_{A,k}$ and $S^v_{B,k}$ are the scattering matrices centered at u and v. Then*

$$S^v_{B,k} = T^{-1} \cdot S^u_{A,k} \cdot T, \tag{64}$$

where $T : \ell^2 \mapsto \ell^2$ is defined by the formula

$$T = F \cdot e^{ik[(y_2 - y_1) \cdot \cos(\theta) - (x_2 - x_1) \cdot \sin(\theta)]} \cdot F^{-1}, \tag{65}$$

where the function

$$\Gamma(\theta) = e^{ik[(y_2 - y_1) \cdot \cos(\theta) - (x_2 - x_1) \cdot \sin(\theta)]} \tag{66}$$

is regarded as the diagonal linear mapping $\Gamma : L^2[0, 2\pi] \mapsto L^2[0, 2\pi]$ defined by the formula

$$(\Gamma \cdot f)(\theta) = \Gamma(\theta) \cdot f(\theta), \tag{67}$$

for all $f \in L^2[0, 2\pi]$.

Remark 2.23 *Since Γ and therefore T are orthogonal mappings, two scattering matrices corresponding to the same scatterer but centered differently are connected to each other by orthogonal transforms; therefore, the two scattering matrices contain the same amount of information about the scatterer.*

2.5 The Near Field

Given $r > 0$ and an incident field ϕ_0 upon the chopped scatterer $q_{D(r)}$, the scattered field ψ is smooth inside $D(r)$, continuous across the circle $|x| = r$, and is of the form (see (23))

$$\psi(\rho, \theta) = \sum_{m=-\infty}^{\infty} \beta_m \cdot H_m(k\rho) \cdot e^{im\theta}, \tag{68}$$

11

outside $D(r)$. The series (68) is absolutely convergent for $\rho > r$. We refer to $\psi|_{\rho=r}$ as the near field. In this subsection, we estimate the rate of convergence of (68) at $\rho = r$.

Lemma 2.24 *Suppose that r is a positive number and that the scatterer q is smooth on $\overline{D(r)}$. Suppose further that $\psi : R^2 \to C$ is the scattered field corresponding to an incident field $\phi_0 : D(r) \to C$ upon the chopped scatterer $q_{D(r)}$. Then the near field $\psi|_{\rho=r}$ has the Fourier series*

$$\psi(r, \theta) = \sum_{m=-\infty}^{\infty} b_m \cdot e^{im\theta}. \tag{69}$$

Furthermore, given r, k, q, there exists $c > 0$, such that

$$b_m \leq \frac{c\|\phi_0\|_2}{m^2}, \tag{70}$$

for all $|m| \geq N_0(kr)$.

Proof. It is well-known (see [6]) that the scattered field is the solution of the Lippmann-Schwinger equation

$$\psi(x) + k^2 \int_{D(r)} G_k(x, \xi) q(\xi) \psi(\xi) d\xi = -k^2 \int_{D(r)} G_k(x, \xi) q(\xi) \phi_0(\xi) d\xi, \tag{71}$$

that it is smooth on $\overline{D(r)}$, and that, given r, k, q, there exists $c_1 > 0$ such that

$$\|\psi\|_\infty \leq c_1 \|\phi_0\|_2. \tag{72}$$

It is also well-known that (see [1], [3]) the free space Green's function G_k can be expressed as

$$G_k(x, \xi) = -\frac{i}{4} \sum_{m=-\infty}^{\infty} H_m(k\rho) J_m(k\varrho) e^{im(\theta-\vartheta)}, \tag{73}$$

with $x = \rho(\cos(\theta), \sin(\theta))$, $\xi = \varrho(\cos(\vartheta), \sin(\vartheta))$. Therefore, the charge density $\sigma : \overline{D(r)} \to C$ defined by the formula

$$\sigma(x) = -k^2 q(x)(\psi(x) + \phi_0(x)), \tag{74}$$

is a smooth function, and that, given r, k, q, there exists $c_2 > 0$ such that

$$\|\sigma\|_\infty \leq c_2 \|\phi_0\|_2. \tag{75}$$

It follows from (71) and (74) that

$$\psi(x) = \int_{D(r)} G_k(x, \xi) \sigma(\xi) d\xi. \tag{76}$$

12

For $x = \rho(\cos(\theta), \sin(\theta))$ and $\rho > r$, the substitution of (73) into (76) yields

$$\psi(\rho, \theta) = -\frac{i\pi}{2} \sum_{m=-\infty}^{\infty} \left(\int_0^r a_m(\varrho) \cdot J_m(k\varrho) \cdot \varrho \cdot d\varrho \right) H_m(k\rho) e^{im\theta}, \qquad (77)$$

where

$$a_m(\varrho) = \frac{1}{2\pi} \int_0^{2\pi} \sigma(\varrho, \vartheta) e^{-im\vartheta} d\vartheta \qquad (78)$$

is the m-th Fourier mode of σ on the circle $|x| = \varrho$. Therefore, according to (75), there exists $c_3 > 0$ such that

$$|a_m(\varrho)| \leq c_3 \|\phi_0\|_2, \qquad (79)$$

for all integer m and real $\varrho \in [0, r]$. Let

$$b_m = -\frac{i\pi}{2} \int_0^r a_m(\varrho) \cdot J_m(k\varrho) \cdot H_m(kr) \cdot \varrho \cdot d\varrho. \qquad (80)$$

Then

$$|b_m| \leq \frac{c_3 \cdot \pi \|\phi_0\|_2}{2} \int_0^r |J_m(k\varrho) \cdot H_m(kr)| \cdot \varrho \cdot d\varrho. \qquad (81)$$

For $m \geq N_0(kr)$, according to (13) and (14), there exists a positive number c_4 such that

$$|J_m(k\varrho) \cdot H_m(kr)| \leq \frac{c_4}{m} \cdot \left(\frac{\varrho}{r} \right)^m. \qquad (82)$$

It follows immediately from (81) and (82) that

$$|b_m| \leq \frac{c_3 \cdot c_4 \cdot \pi \|\phi_0\|_2}{2} \cdot \frac{1}{m^2}. \qquad (83)$$

Now, letting $\rho \to r$ in (77) and combining the result with (80) and (83), we obtain (69) and (70). $\square$

Remark 2.25 *For $|m| \leq z$, it is well-known (see [3], pp 366) that*

$$J_m(z) = O\left(\frac{1}{z^{1/3}} \right), \qquad (84)$$

$$H_m(z) = O\left(\frac{1}{z^{1/3}} \right). \qquad (85)$$

It follows from (79) and (80) that

$$|b_m| \leq c_3 \|\phi_0\|_2 \frac{1}{(kr)^{2/3}}, \qquad (86)$$

for all $|m| \leq kr$. This means that as a function of m, the Fourier coefficients $\{b_m\}$ of (69) remain flat in magnitude for $|m| \leq kr$. The magnitude begins to decrease quite suddenly when $|m|$ becomes greater than kr; it decays to zero at the rate $1/m^2$ for $m \geq N_0(kr)$.

In Lemma 2.24, choose

$$\phi_0(\rho, \theta) = J_n(k\rho) \cdot e^{in\theta}, \tag{87}$$

then it follows from (22)—(24) that the Fourier coefficients $\{\, b_m, -\infty < m < \infty \,\}$ of the near field $\psi|_{\rho=r}$, are same as the entries of the the n-th column of the matrix $H_{kr} \cdot S_{r,k}$. In other words,

$$b_m = (H_{kr} \cdot S_{r,k})_{m,n}. \tag{88}$$

The following lemma is a restatement of Lemma 2.24 in terms of the scattering matrix.

Lemma 2.26 *Suppose that r is a positive number and that the scatterer q is smooth on $\overline{D(r)}$. Suppose further that $S_{r,k}$ is the scattering matrix corresponding to the chopped scatterer $q_{D(r)}$. Then there exists a positive number c such that*

$$|(H_{kr} \cdot S_{r,k})_{m,n}| \le \frac{c}{m^2}, \tag{89}$$

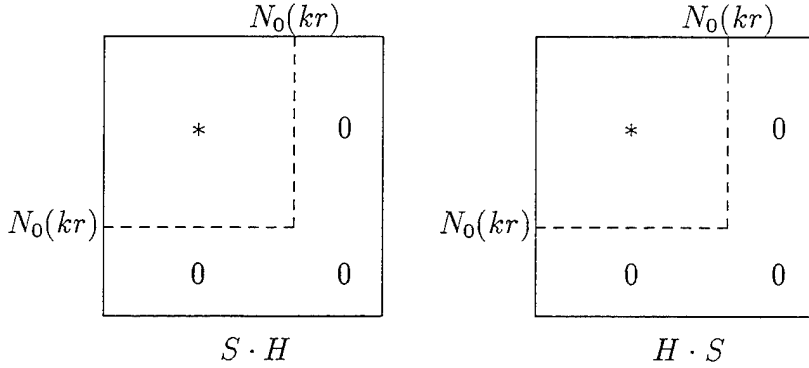*uniformly for all integers n and m such that $|m| \ge N_0(kr)$.*

Figure 3: Structures of the Matrices $S_{r,k} \cdot H_{kr}$, $H_{kr} \cdot S_{r,k}$.

The following remark is a restatement of Remark 2.25 in terms of the scattering matrix.

Remark 2.27 *When m becomes greater in absolute value than kr, the elements on the m-th row of $H_{kr} \cdot S_{r,k}$ begin to decrease; they decay uniformly at the rate $1/m^2$ for $m \ge N_0(kr)$. If we omit the small entries in the part of the matrix $H_{kr} \cdot S_{r,k}$ whose row index m is greater than $N_0(kr)$ in absolute value, it follows from Remark 2.14 that $H_{kr} \cdot S_{r,k}$ is approximately a square matrix of dimension $2 \cdot N_0(kr)$ (see Figure 3). It follows immediately from Lemmas 2.17 and 2.18 that*

$$(S_{r,k} \cdot H_{kr})^\tau = \Upsilon \cdot H_{kr} \cdot S_{r,k}. \tag{90}$$

Therefore, $(S_{r,k} \cdot H_{kr})^\tau$ is approximately a square matrix of dimension $2 \cdot N_0(kr)$, and so is $S_{r,k} \cdot H_{kr}$.

Figure 3 shows the structures of the two matrices $S_{r,k} \cdot H_{kr}$ and $H_{kr} \cdot S_{r,k}$; compare with Figure 2. Only the first quadrant of the matrices (entries with both row and column indices positive) is depicted here. In the figure, the section of a matrix labeled zero have entries small compared to entries in the square submatrix of dimension $2 \cdot N_0(kr)$.

2.6 Continuation Method for Nonlinear Problem

For simplicity, we will restrict our discussion to the case of finite dimensional space. Let us consider a nonlinear mapping $P : R^n \times [0,1] \mapsto R^n$ and the solution of the problem

$$P(x, 1) = 0. \tag{91}$$

Suppose that for every $\lambda \in [0,1]$, there exists a unique solution $x_\lambda \in R^n$ to the problem

$$P(x_\lambda, \lambda) = 0. \tag{92}$$

Suppose further that x_λ depends smoothly on λ, and that the mapping P is smooth. Finally, suppose that x_0 is known. Then there is a procedure referred to as the continuation method which obtains the solution x_1 using the "initial solution" x_0, by recursively solving a series of linearized problems. This simple scheme is as follows.

Suppose that at some $\lambda \in [0,1)$ we have obtained the solution x_λ. For a sufficiently small $h > 0$, we intend to obtain $x_{\lambda+h}$, the solution of the equation

$$P(x_{\lambda+h}, \lambda + h) = 0. \tag{93}$$

Subtracting (92) from (93), we have

$$\left\{ \frac{\partial P(x_\lambda, \lambda)}{\partial x} \right\} \cdot (x_{\lambda+h} - x_\lambda) = -h \frac{\partial P(x_\lambda, \lambda)}{\partial \lambda} + O(h^2). \tag{94}$$

In other words, up to the second order of h, the perturbation

$$\delta x = x_{\lambda+h} - x_\lambda \tag{95}$$

is a solution of a linear problem. If we further assume that the $n \times n$ matrix

$$\frac{\partial P(x_\lambda, \lambda)}{\partial x} \tag{96}$$

is not singular, the increment δx can be determined up to second order of h.

Remark 2.28 *In most applications, once the second order approximation of $x_{\lambda+h}$ is obtained, no further attempt is made to compute the exact $x_{\lambda+h}$. Instead, the recursion in λ proceeds to compute the next solution $x_{\lambda+2h}$ from the approximate solution $x_{\lambda+h}$ just obtained.*

Obviously, the linearization procedure is a standard perturbation analysis on the parameter λ. Sometimes, it is more convenient and advantageous, both computationally and analytically, to carry out the perturbation analysis in a slightly different way. Suppose we do not wish to evaluate the term

$$\frac{\partial P(x_\lambda, \lambda)}{\partial \lambda} \tag{97}$$

on the right hand side of (94). Given x_λ, let us compute

$$\epsilon = P(x_\lambda, \lambda + h). \tag{98}$$

Subtracting (98) form (93), we obtain

$$\left\{ \frac{\partial P(x_\lambda, \lambda + h)}{\partial x} \right\} \cdot \delta x = -\epsilon + O(h^2). \tag{99}$$

It is easy to verify that ϵ is of order h. As before, a second order approximation of the solution $x_{\lambda+h}$ can be obtained from x_λ by solving a linear problem.

2.7 The Solution of a Linear ODE of Matrix

Suppose that $A(r)$, $B(r)$ and $C(r)$ are three $n \times n$ matrices depending continuously on $r \in [0,1]$. Let us consider an ordinary differential equation of the form

$$S'(r) = A(r) \cdot S(r) + S(r) \cdot B(r) + C(r). \tag{100}$$

Now, we wish to express in close form the solution $S(r)$ at an arbitrary $r \in (0,1]$ for prescribed initial value $S(0)$.

Lemma 2.29 *Suppose that the $n \times n$ matrix $P(r)$ is continuous for all $r \in [0,1]$. Suppose further that $a < b$ are two real numbers in $[0,1]$. Finally suppose that m is a positive integer, and that $h = (b-a)/m$. Then the two limits*

$$
\begin{aligned}
E_L(a,b;P) &= \lim_{m \to \infty} (I + h \cdot P(b))(I + h \cdot P(b-h)) \times \ldots \times \\
&\qquad (I + h \cdot P(a+h))(I + h \cdot P(a)), \tag{101} \\
E_R(a,b;P) &= \lim_{m \to \infty} (I + h \cdot P(a))(I + h \cdot P(a+h)) \times \ldots \times \\
&\qquad (I + h \cdot P((b-h)))(I + h \cdot P(b)) \tag{102}
\end{aligned}
$$

exist. Moreover, for arbitrary real numbers r_1, r_2, $r_3 \in [0,1]$,

$$
\begin{aligned}
E_L(r_1, r_3; P) &= E_L(r_2, r_3; P) E_L(r_1, r_2; P), \tag{103} \\
E_R(r_1, r_3; P) &= E_R(r_1, r_2; P) E_R(r_2, r_3; P). \tag{104}
\end{aligned}
$$

Finally,

$$\frac{\partial E_L(a, b; P)}{\partial a} = E_L(a, b; P) \cdot P(a), \tag{105}$$

$$\frac{\partial E_L(a, b; P)}{\partial b} = P(b) \cdot E_L(a, b; P), \tag{106}$$

$$\frac{\partial E_R(a, b; P)}{\partial a} = P(a) \cdot E_R(a, b; P), \tag{107}$$

$$\frac{\partial E_R(a, b; P)}{\partial b} = E_R(a, b; P) \cdot P(b). \tag{108}$$

The proof of Lemma 2.29 is trivial, and is omitted here.

Remark 2.30 *If, for any real numbers c, $d \in [0, 1]$, $P(c)$ commutes with $P(d)$, then*

$$E_L(a, b; P) = E_R(a, b; P) = \exp\left(\int_a^b P(r)dr\right). \tag{109}$$

Remark 2.31 *Under the conditions of the preceding lemma, it can be easily shown that*

$$
\begin{aligned}
E_L(a, b; P) &= \left(I - \frac{h}{2}P(b)\right)^{-1} \left(I + \frac{h}{2}P(b - h)\right) \times \\
&\quad \left(I - \frac{h}{2}P(b - h)\right)^{-1} \left(I + \frac{h}{2}P(b - 2h)\right) \times \ldots \times \\
&\quad \left(I - \frac{h}{2}P(a + h)\right)^{-1} \left(I + \frac{h}{2}P(a)\right) + O(h^2),
\end{aligned} \tag{110}
$$

and

$$
\begin{aligned}
E_R(a, b; P) &= \left(I + \frac{h}{2}P(a)\right) \left(I - \frac{h}{2}P(a + h)\right)^{-1} \times \\
&\quad \left(I + \frac{h}{2}P(a + h)\right) \left(I - \frac{h}{2}P(a + 2h)\right)^{-1} \times \ldots \times \\
&\quad \left(I + \frac{h}{2}P(b - h)\right) \left(I - \frac{h}{2}P(b)\right)^{-1} + O(h^2).
\end{aligned} \tag{111}
$$

The following lemma is an immediate consequence of the preceding one.

Lemma 2.32 *Suppose that $A(r)$, $B(r)$ and $C(r)$ are three $n \times n$ matrices depending continuously on $r \in [0, 1]$. Then*

$$S(r) = \int_0^r E_L(\tau, r; A) \cdot C(\tau) \cdot E_R(\tau, r; B) \cdot d\tau \tag{112}$$

is the solution of the initial value problem

$$S'(r) = A(r) \cdot S(r) + S(r) \cdot B(r) + C(r), \qquad (113)$$
$$S(0) = 0. \qquad (114)$$

3 Heisenberg's Uncertainty Principle and Recursive Linearization

It turns out that the ill-posedness of the inverse scattering problem can be beneficially used to solve it. It means that, due to ill-posedness of the problem, not all equations in the nonlinear system (see Remark 2.15) are strongly nonlinear, and that when solved recursively in a proper order, they can be reduced to a collection of linear problems. In this section, we reformulate the ill-posedness and the inverse scattering problem, and present an inversion algorithm. More specifically, in Section 3.1, we examine and reformulate the ill-posedness of the inverse scattering problem in the special case of weak scattering. In Section 3.2, we briefly and informally describe the recursive linearization method. In Section 3.3, we present the Heisenberg's Uncertainty Principle for the scattering problem, which we shall use in Section 3.4 to reformulate the inverse problem. The details of the inversion algorithm will be described in Section 3.6.

3.1 A Special Case

When q or k is small, the scattered field is weak, and the inverse scattering problem becomes essentially linear. In this subsection, we examine this special case and make necessary connections to the general case where the inverse problem is nonlinear.

Nowhere does the ill-posedness of the inverse scattering problem become more manifest than in the case of weak scattering. As is well-known (see, for example, [8], [12]), when $q \ll 1$ or $k \ll 1$, the scattered field is weak, where the Born Approximation to the far field $\psi_\infty(\theta, \beta)$ (see Section 2.4) can be written in the form

$$\psi_\infty(\theta, \beta) = \frac{ik^2}{4} \int_\Omega q(x, y) e^{ik\{x(\cos\beta - \cos\theta) + y(\sin\beta - \sin\theta)\}} dx dy \qquad (115)$$

with an error of $O(q^2)$ if q is small, or of $O(k^4 \log^2(k))$ if k is small. In other words, under the assumption of weak scattering, the far field $\psi_\infty(\theta, \beta)$ depends on q essentially linearly, and, up to a higher order error and a scaling, is the Fourier transform of q

$$\hat{q}_{m,n} = \frac{1}{2\pi} \int_\Omega q(x, y) e^{ik(mx + ny)} dx dy \qquad (116)$$

18

with the pair of real numbers m and n given by

$$m = k(\cos\beta - \cos\theta), \tag{117}$$

$$n = k(\sin\beta - \sin\theta). \tag{118}$$

Therefore, the full-aperture far-field measurements

$$\{\ \psi_\infty(\theta, \beta),\ \ \text{for all}\ \ (\theta, \beta) \in [0, 2\pi] \times [0, 2\pi]\ \} \tag{119}$$

are the Fourier transform $\hat{q}_{m,n}$ for those points (m, n) filling the entire disk $D(2k)$, which we refer to as the Fourier aperture of radius $2k$ (see Definition 2.4 and Figure 5). With such measurements, the scatterer q can be determined, obviously, with the resolution

$$\sigma = \frac{2\pi}{\text{radius of Fourier aperture}} = \frac{2\pi}{2k} = \frac{1}{2}\lambda, \tag{120}$$

where

$$\lambda = \frac{2\pi}{k} \tag{121}$$

is the wavelength. We consequently have

Lemma 3.1 *(Uncertainty Principle, Small q) Suppose that q is small. Then from the far-field measurements, we cannot determine features of the scatterer that are less than half a wavelength.*

Remark 3.2 *Lemma 3.1 is a reformulation of the ill-posedness of the (linear) inverse problem. It explicitly specifies the null space of the linear operator (115) which maps the scatterer q to the scattering measurements ψ_∞: the Fourier modes of q higher than $2k$ are not observable in the measurements, and thus cannot be determined.*

Remark 3.3 *Formulae (115)—(121) are also valid for small k; therefore, Lemma 3.1 implies that at a sufficiently low frequency only $\hat{q}(0, 0)$ (the average of the scatterer) can be determined from the measurements.*

The scattering matrix $S_{r,k}$ is small if scattering is weak. Thus, for small q or small k, the Riccati equation (34) can be linearized by omitting terms from the right hand side of (34) quadratic and cubic in q and $S_{r,k}$. The solution of the linearized equation

$$\frac{dS^B_{r,k}}{dr} = \frac{i\pi r}{2}k^2 \cdot J_{kr} \cdot \hat{q}_r \cdot J_{kr} \tag{122}$$

is given by the formula

$$S^B_{\varpi,k} = \frac{i\pi k^2}{2} \int_0^\varpi J_{kr} \cdot \hat{q}_r \cdot J_{kr} \cdot r \cdot dr. \tag{123}$$

19

Since $S_{\varpi,k}^B$ is an approximation to the scattering matrix $S_{\varpi,k}$, it should be connected to the Born Approximation (115) due to formula (58). The following is a restatement of Lemmas 2.18 of [11] in terms of the scattering matrix.

Lemma 3.4 *Suppose that $S_{r,k}^B$ is the solution of (122), $S_{r,k}$ is the solution of the Riccati equation (34). Then there exists a constant $c > 0$, such that for $k > 0$ and all $r \in [0, \varpi]$,*

$$\|S_{r,k} - S_{r,k}^B\|_2 \le c \cdot (k \cdot |\log(k)| \cdot \|q\|_\infty)^2 . \tag{124}$$

Moreover,

$$F_\theta^{-1} \cdot \Lambda^{-1} \cdot S_{\varpi,k}^B \cdot \Lambda \cdot F_\beta = \int_\Omega q(x,y) e^{ik\{x(\cos\beta - \cos\theta) + y(\sin\beta - \sin\theta)\}} dx dy. \tag{125}$$

3.2 The Inversion Algorithm, An Informal Description

Let us denote by

$$P(q,k) = S_{\varpi,k} \tag{126}$$

the system of nonlinear equations for the inverse scattering problem. In this subsection, we briefly describe a simple procedure that solves the inverse problem.

For a given precision $\epsilon > 0$ and frequency $k > 0$, there should be infinite number of forward models q that satisfies (126) to the prescribed precision, due to the ill-posedness of the problem. We choose from them the most smooth one and denote it by q_k. Therefore, to the given precision, the inverse problem can be reformulated as

$$P(q_k, k) = S_{\varpi,k}. \tag{127}$$

We expect that q_k lives in a finite dimensional subspace of L^2, just as it is the case when q is sufficiently small: the Fourier transform of q_k is essentially zero outside the disk $D(2k)$ (see Remark 3.2). The inversion algorithm is a recursive linearization procedure which recovers q_k from small k to large k.

For sufficiently small k, according to Remark 3.3, q_k lives in a one-dimensional subspace; it is the average of q. Moreover, the equation (127) is linear to the prescribed precision ϵ, and therefore can be solved in the least-squares sense to obtain q_k.

Now suppose that q_k depends continuously on k, and that we have recovered q_k at some $k > 0$. Then the standard procedure of continuation (see Section 2.6) can be used to recover $q_{k+\delta k}$ by solving a linear problem for the perturbation

$$\delta q = q_{k+\delta k} - q_k. \tag{128}$$

Consequently, the inverse scattering problem (126) can be solved up to any given frequency k and to the prescribed precision $\epsilon > 0$, provided that the scattering data (20) are available.

20

In the next several subsections, we characterize more precisely the finite dimensional subspace in which q_k resides, and describe the inversion algorithm in detail.

3.3 Uncertainty Principle, the General Case

According to Lemma 3.4, when q is small and up to the second order of the smallness, the knowledge of the scattering data $S_{\varpi,k}$ is equivalent to the knowledge of the Fourier modes of q in the aperture $D(2k)$. It turns out that when q is not small, the above statement still essentially holds. In other words, $S_{\varpi,k}$ contains information of the Fourier modes of q essentially in $D(2k)$. In this subsection, we wish to make this assertion more precise, and to show it is indeed the case.

In the evaluation of the right hand side of the Riccati equation (34), $J_{kr} + S_{r,k}{\cdot}H_{kr}$, $H_{kr}{\cdot}S_{r,k} + J_{kr}$, according to Remarks 2.13 and 2.27, essentially are two square matrices of size $2{\cdot}N_0(kr)$. Therefore, the operation

$$(J_{kr} + S_{r,k}{\cdot}H_{kr}){\cdot}\hat{q}_r{\cdot}(H_{kr}{\cdot}S_{r,k} + J_{kr}) \tag{129}$$

on $\hat{q}_r$ (see (33)) is a process of low-pass filtering on the scatterer q, as depicted in Figure 4. At a given frequency k and on the circle $|x| = r$, only the Fourier modes

$$\{ \ \hat{q}_m(r) \ \mid \ |m| < 2{\cdot}N_0(kr) \ \} \tag{130}$$

essentially participate in the operation; higher-frequency modes of the scatterer are filtered out in the process. The relatively low-frequency angular Fourier coefficients (130) at r are therefore picked up in the integration

$$S_{\varpi,k} = \frac{i\pi k^2}{2} \int_0^\varpi (J_{kr} + S_{r,k}{\cdot}H_{kr}){\cdot}\hat{q}_r{\cdot}(H_{kr}{\cdot}S_{r,k} + J_{kr}){\cdot}r{\cdot}dr, \tag{131}$$

and encoded in the scattering data $S_{\varpi,k}$. We thus conclude that the scattering data contain insignificant information of the higher-frequency angular Fourier coefficients

$$\{ \ \hat{q}_m(r) \ \mid \ |m| \geq 2{\cdot}N_0(kr) \ \} \tag{132}$$

of the scatterer for all $r \in [0, \varpi]$. In other words, at each $r > 0$, the resolution of the scatterer on the circle $|x| = r$ is

$$\frac{2\pi r}{2N_0(kr)} \approx \frac{\pi}{k} = \frac{1}{2}\lambda. \tag{133}$$

That is, the angular resolution is about half a wavelength. Features of q smaller than half a wavelength in the angular direction contribute considerably weakly to the scattering data; the smaller the features become, the weaker the contributions are, and the more difficult it becomes to recover these small features. The above discussion can be summarized in the following lemma.
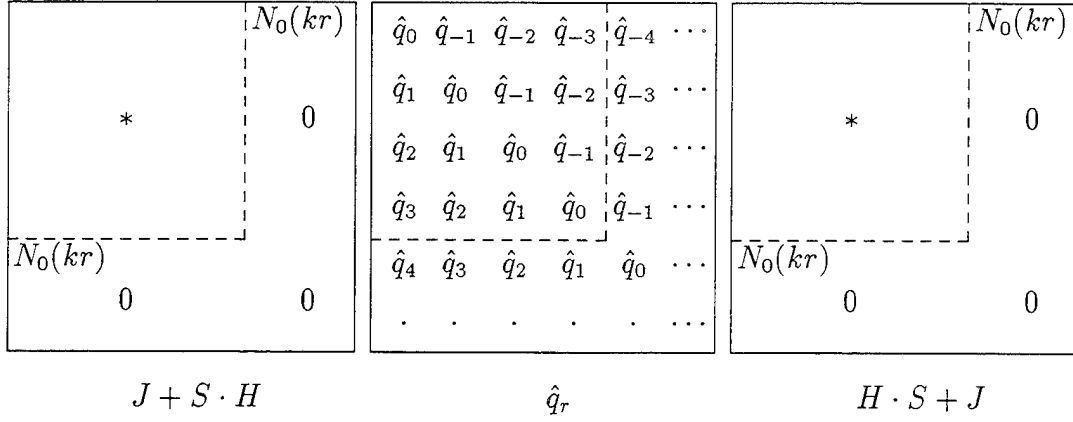
21

$$
\begin{array}{|ccccccc|}
\hline
& & & & \vdots\,N_0(kr) \\
\ast & & & & \quad\ 0 \\
& & & & \\
\hline
N_0(kr) & & & & \\
\quad\ 0 & & & & \ 0 \\
\hline
\end{array}
\qquad
\begin{array}{ccccccc}
\hat{q}_0 & \hat{q}_{-1} & \hat{q}_{-2} & \hat{q}_{-3} & \hat{q}_{-4} & \cdots \\
\hat{q}_1 & \hat{q}_0 & \hat{q}_{-1} & \hat{q}_{-2} & \hat{q}_{-3} & \cdots \\
\hat{q}_2 & \hat{q}_1 & \hat{q}_0 & \hat{q}_{-1} & \hat{q}_{-2} & \cdots \\
\hat{q}_3 & \hat{q}_2 & \hat{q}_1 & \hat{q}_0 & \hat{q}_{-1} & \cdots \\
\hat{q}_4 & \hat{q}_3 & \hat{q}_2 & \hat{q}_1 & \hat{q}_0 & \cdots \\
\cdot & \cdot & \cdot & \cdot & \cdot & \cdots
\end{array}
\qquad
\begin{array}{|ccccccc|}
\hline
& & & & \vdots\,N_0(kr) \\
\ast & & & & \quad\ 0 \\
& & & & \\
\hline
N_0(kr) & & & & \\
\quad\ 0 & & & & \ 0 \\
\hline
\end{array}
$$

$$J + S \cdot H \qquad\qquad \hat{q}_r \qquad\qquad H \cdot S + J$$

Figure 4: Process of Low-pass Filtering of the Scatterer.

Lemma 3.5 *(Uncertainty Principle, Angular Direction) Suppose that the smooth scatterer q has compact support $D(\varpi)$, and that $S_{\varpi,k}$ is the corresponding scattering matrix. Then it is increasingly difficult to determine from $S_{\varpi,k}$ small features of q in the angular direction as their sizes become increasingly less than half a wavelength.*

Now, we show that the resolution of the scatterer in an arbitrary direction is also about half a wavelength. Given $\xi = (a, b) \in R^2$, let $A = \varpi + |\xi|$, and consider the scattering matrix $S^{\xi}_{A,k}$, centered at ξ and corresponding to the scatterer q (see Section 2.4). According to Remark 2.23, $S^{\xi}_{A,k}$ and the scattering data $S_{\varpi,k}$ contain the same amount of information about the scatterer; therefore $S^{\xi}_{A,k}$ can be used as the scattering data to recover the same scatterer, now represented by the function $q^{\xi}(x,y) = q(x - a, y - b)$. According to Lemma 3.5, the angular resolution provided by the scattering data $S^{\xi}_{A,k}$ is about half a wavelength. In other words, the resolution of q^{ξ} on any circle centered at ξ is about half a wavelength. Therefore, for a given point x inside the scatterer and for a given direction $\vec{\tau}$, we can always choose the center ξ which is sufficiently far from the location of the scatterer, such that there is one circle centered at ξ which passes through x in direction $\vec{\tau}$. Since the resolution of the scatterer on this circle is about half a wavelength, and since $S^{\xi}_{A,k}$ contains the same amount of information about q as the original scattering data $S_{\varpi,k}$ does, we obtain:

Lemma 3.6 *(Uncertainty Principle) Suppose that the smooth scatterer q has compact support $D(\varpi)$, and that $S_{\varpi,k}$ is the corresponding scattering matrix. Then it is increasingly difficult to determine from $S_{\varpi,k}$ small features of q as their sizes become increasingly less than half a wavelength. In other words, contained in the measurements $S_{\varpi,k}$ are essentially the Fourier modes of q inside the Fourier aperture $D(N_0(2k))$.*

Denote by $D(2k)^+$ the Fourier aperture where the Fourier modes of q can be recovered from the measurements $S_{\varpi,k}$ in a well-conditioned procedure. Presently, no detailed characterization of $D(2k)^+$ is available except that it belongs to $D(N_0(2k))$.
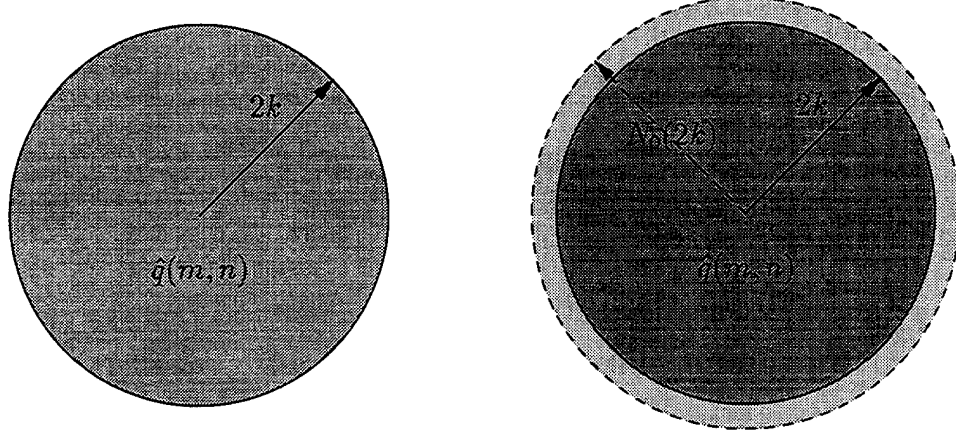

Figure 5: Fourier apertures $D(2k)$ and $D(2k)^+$.

Remark 3.7 *The Uncertainty Principle is an equivalent formulation of the ill-posedness of the inverse scattering problem: small features of the scatterer belong to the virtually-null space (see Remark 2.12) of the nonlinear mapping of the inverse scattering problem; they are essentially not observable in a scattering experiment.*

3.4 Reformulating Scattering Problem

Denote by q_k the low-frequency part of q in the Fourier aperture $D(2k)^+$, so that

$$\widehat{(q_k)}_{m,n} = \begin{cases} \hat{q}_{m,n}, & (m,n) \in D(2k)^+, \\ 0, & (m,n) \notin D(2k)^+. \end{cases} \tag{134}$$

The goal of inversion, in the lights of Lemma 3.6, is to stably obtain q_k within a reasonable precision. By definition, q_k is the only component of q that is observable in the scattering data; consequently the original forward scattering model q can be replace by q_k without (essentially) changing the measurements. We therefore can reformulate the equation (34) as

$$\frac{dS_{r,k}}{dr} = \frac{i\pi r}{2} k^2 (J_{kr} + S_{r,k} \cdot H_{kr}) \cdot \widehat{(q_k)}_r \cdot (H_{kr} \cdot S_{r,k} + J_{kr}). \tag{135}$$

Definition 3.8 *To a scattering experiment at frequency k, a scatterer $\check{q}$ is said to look (essentially) the same as a scatterer $\check{q}$ if they produce essentially the same scattering measurements in the experiment.*

Definition 3.9 *A forward model $\tilde{q}$ is said to be observable, or an observable part of the original scatterer q, to a scattering experiment at frequency k, if it looks the same as the original q, and its L^2 norm is the least among those that look the same as q.*

Remark 3.10 *At frequency k, q_k looks the same as the original q to a full-aperture experiment, it is also observable to the full-aperture experiment. On the other hand, in an experiment of limited aperture, q_k may not be the observable forward model, but it looks the same as the observable.*

3.5   Continuity of q_k in Frequency k

In this subsection, we argue that q_k, the observable part of q at frequency k, depends on k continuously. This is certainly true in the special case of small q. There, the observable part of q is the Fourier modes of q in aperture $D(2k)$ (see Section 3.1). Therefore, new Fourier modes added to $q_{k+\delta k}$ are those $\hat{q}_{m,n}$ in the annulus

$$A(k, \delta k) = \{ \ (m, n), \ 2k \le \sqrt{m^2 + n^2} \le 2(k + \delta k) \ \}. \tag{136}$$

Consequently, the perturbation in q_k, due to the small perturbation in k, is small:

$$\|q_{k+\delta k} - q_k\|_2 = \|\widehat{q_{k+\delta k}} - \widehat{q_k}\|_2 = \int_{A(k,\delta k)} \hat{q}_{m,n} \cdot dm \cdot dn = O(\delta k). \tag{137}$$

Assuming the well-posedness of the initial value problem (see (34), (26)) of the Riccati equation, we further argue that the dependence of q_k on k is also continuous in the general case where q is not small. This well-posedness means, in particular, that the scattering matrix $S_{r,k}$ is a smooth function of k, that its virtual rank and structure of essentially nonzero entries (see Figure 1) depend on k smoothly. Therefore the amount of information the process (129) acquires from q depends on k smoothly. We summarize the above discussion as an Observation for later reference.

Observation 3.11 *To a full-aperture experiment, the observable scattering model q_k depends continuously on k in the L^2 norm.*

We wish to carry this point further to the case of limited-aperture measurements. Denote by $q_{k,l}$ the observable part of q corresponding to an experiment of a limited aperture. Usually, $q_{k,l}$ is not the same as q_k, and therefore, due to Definition 3.9,

$$\|q_{k,l}\|_2 < \|q_k\|_2. \tag{138}$$

We postulate that Observation 3.11 is also valid for scattering experiments with limited aperture. This has been observed in our numerical experiments, and can be proved, again, in the special case of small q.

3.6 A Recursive Linearization Algorithm

Suppose that a set of full-aperture, full-bandwidth scattering data (see (20)) are given, we present in this subsection a stable method for the solution of the inverse scattering problem. There are two approaches to the description of the method: one is based on the Lippmann-Schwinger equation (see [12]), the other on the Riccati equation, which has been numerically implemented (see Section 4), and which we wish to present here.

Let us again consider the nonlinear mapping (see Remark 2.15) which maps the scatterer q to the scattering data (see (20))

$$\{\, S_{\varpi,k} \mid 0 < k < \infty \,\}, \tag{139}$$

defined by the initial value problem (see Section 3.4 and (26))

$$S'_{r,k} = \frac{i\pi r}{2} k^2 (J_{kr} + S_{r,k} \cdot H_{kr}) \cdot \widehat{(q_k)}_r \cdot (H_{kr} \cdot S_{r,k} + J_{kr}), \tag{140}$$

$$S_{0,k} = 0. \tag{141}$$

Discretizing the k-variable with nodes k_1, k_2, k_3, ... (see Figure 6), we now describe a procedure which recursively determines q_k at $k = k_j$ for $j = 1, 2, \ldots$ Indeed, for sufficiently small k_1, the relationship between q_{k_1} and S_{r,k_1} becomes
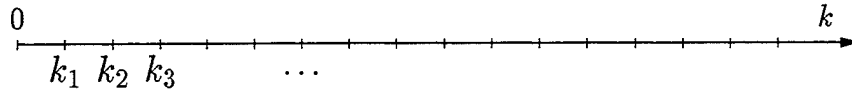

Figure 6: Computational Grid in the Frequency Space.

essentially linear (see Section 3.1), and the problem (140), (141) can be replaced by the linear one (see Lemma 3.4):

$$S'_{r,k_1} = \frac{i\pi r}{2} k_1^2 \cdot J_{k_1 r} \cdot \widehat{(q_{k_1})}_r \cdot J_{k_1 r} \tag{142}$$

$$S_{0,k_1} = 0 \tag{143}$$

The solution to this linear initial value problem is obviously given by the formula

$$S_{\varpi,k_1} = \frac{i\pi k_1^2}{2} \int_0^{\varpi} J_{k_1 r} \cdot \widehat{(q_{k_1})}_r \cdot J_{k_1 r} \cdot r \cdot dr. \tag{144}$$

Now, for the given scattering data S_{ϖ,k_1}, the scatterer q_{k_1} can be obtained by solving the linear problem (144).

Remark 3.12 *In practice, only an approximate q_{k_1} is needed to start the recursive procedure, namely, to determine q_{k_2}. Therefore, k_1 can usually be chosen*

quite large, and consequently, the linear equation (142) is not a fine approximation to the Riccati equation (140). We find in numerical experiments that the lowest frequency k_1 can be chosen such that its corresponding wavelength is about the size of the scatterer.

By induction, suppose that the scatter $q_{\tilde{k}}$ have heen recovered at some $\tilde{k} > 0$, and
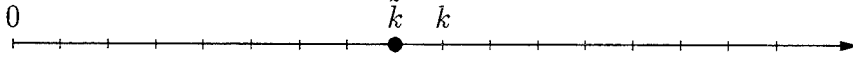

Figure 7: Update from $\tilde{k}$ to k.

that $k > 0$ is slightly greater than $\tilde{k}$. We intend to determine q_k, or equivalently, to determine the perturbation

$$\delta q = q_k - q_{\tilde{k}}. \tag{145}$$

This can be achieved by employing the perturbation analysis of Section 2.6 where the continuation parameter λ is now the frequency k. Following the procedures described in (98) and (99), we solve at the frequency k the forward scattering problem

$$\check{S}'_{r,k} = \frac{i\pi r}{2} k^2 (J_{kr} + \check{S}_{r,k} \cdot H_{kr}) \cdot \widehat{(q_{\tilde{k}})}_r \cdot (H_{kr} \cdot \check{S}_{r,k} + J_{kr}), \tag{146}$$

$$\check{S}_{0,k} = 0, \tag{147}$$

corresponding to the scatterer $q_{\tilde{k}}$. As a result of the forward solve, we obtain $\check{S}_{r,k}$ for all $r \in [0, \varpi]$, which will be used later in the linearized equations for the perturbation δq (see equations (151), (153)).

Remark 3.13 *On the assumption that the initial value problem of the Riccati equation (see (26), (34)) is well-posed, we observe that the scattering matrix $\check{S}_{r,k}$, the solution of (146) and (147) with the scatterer function $q_{\tilde{k}}$, is different from but close to $S_{r,k}$; for the latter is the solution of the same equations*

$$S'_{r,k} = \frac{i\pi r}{2} k^2 (J_{kr} + S_{r,k} \cdot H_{kr}) \cdot \widehat{(q_k)}_r \cdot (H_{kr} \cdot S_{r,k} + J_{kr}), \tag{148}$$

$$S_{0,k} = 0, \tag{149}$$

with a different scatterer function q_k close to $q_{\tilde{k}}$.

Subtracting (146) from (148), and omitting the second order smallness in δq and in

$$(\delta S)_{r,k} = S_{r,k} - \check{S}_{r,k}, \tag{150}$$

26

we obtain the linear ordinary differential equation

$$
(\delta S)'_{r,k} = \frac{i\pi r}{2}k^2\left\{(J_{kr} + \check{S}_{r,k}\cdot H_{kr})\cdot\widehat{(q_{\check{k}})}_r\cdot H_{kr}\cdot(\delta S)_{r,k} + \right.
$$
$$
+ (\delta S)_{r,k}\cdot H_{kr}\cdot\widehat{(q_{\check{k}})}_r\cdot(H_{kr}\cdot\check{S}_{r,k} + J_{kr}) +
$$
$$
\left. + (J_{kr} + \check{S}_{r,k}\cdot H_{kr})\cdot\widehat{(\delta q)}_r\cdot(H_{kr}\cdot\check{S}_{r,k} + J_{kr})\right\} \tag{151}
$$

for δS, with its initial value

$$
(\delta S)_{0,k} = 0. \tag{152}
$$

According to Lemma 2.32, the linear initial value problem (151), (152) has the formal solution

$$
(\delta S)_{r,k} = \frac{i\pi}{2}k^2\int_0^r E_L(\tau,r;P_y)\cdot(J_{k\tau} + \check{S}_{\tau,k}\cdot H_{k\tau}) \times
$$
$$
\widehat{(\delta q)}_\tau\cdot(H_{k\tau}\cdot\check{S}_{\tau,k} + J_{k\tau})\cdot E_R(\tau,r;P_x)\cdot\tau\cdot d\tau \tag{153}
$$

where $P_x(r) : X_{kr} \mapsto X_{kr}$, $P_y(r) : Y_{kr} \mapsto Y_{kr}$ are defined by the formulae

$$
P_x(r) = \frac{i\pi}{2}k^2 r H_{kr}\cdot\widehat{(q_{\check{k}})}_r\cdot(H_{kr}\cdot\check{S}_{r,k} + J_{kr}), \tag{154}
$$

$$
P_y(r) = \frac{i\pi}{2}k^2 r(J_{kr} + \check{S}_{r,k}\cdot H_{kr})\cdot\widehat{(q_{\check{k}})}_r\cdot H_{kr}. \tag{155}
$$

In particular, at $r = \varpi$, (153) becomes a system of linear equations for $\widehat{\delta q}$:

$$
\frac{i\pi}{2}k^2\int_0^\varpi E_L(r,\varpi;P_y)\cdot(J_{kr} + \check{S}_{r,k}\cdot H_{kr})\cdot\widehat{(\delta q)}_r \times
$$
$$
(H_{kr}\cdot\check{S}_{r,k} + J_{kr})\cdot E_R(r,\varpi;P_x)\cdot r\cdot dr = (\delta S)_{\varpi,k}, \tag{156}
$$

with the right hand sides $(\delta S)_{\varpi,k}$ given, and the coefficients $E_L, E_R, \check{S}$ known. Denote by $L(X_{k\varpi} \mapsto Y_{k\varpi})$ the linear space of all linear mappings from $X_{k\varpi}$ to $Y_{k\varpi}$, and by $\mathcal{L}_k : L^2[D(\varpi)] \mapsto L(X_{k\varpi} \mapsto Y_{k\varpi})$ the linear operator defined by (156). The linear equation (156) can be rewritten as

$$
\mathcal{L}_k(\delta q) = (\delta S)_{\varpi,k}. \tag{157}
$$

The linear equations can be solved (see Remark 3.14) for δq, and the scatterer q_k can be obtained from the previously recovered scatterer $q_{\check{k}}$ via (145).

Remark 3.14 *The virtual rank (see Remark 2.12) of the linear operator $\mathcal{L}_k$ is finite due to the ill-posedness of the inverse scattering problem (see Lemma 3.6 and Remark 3.7). Therefore, (157) is solved as a least-squares problem of finite dimensions to yield the solution δq. Our numerical experiments show that in fact only an roughly approximate q_k is needed to continue the up recursion in k, namely, to stably determine the scatterer at the next higher frequency.*

4 Implementations of the Recursive Procedure

In this section, we discuss the discretization of the spatial variables (r, θ), the treatment of the scattering matrix S, the numerical computation of the Riccati equation (146), the evaluation of the linear operators E_L, E_R, the formation of the linear system (156), and the least-squares solution of it.

4.1 Discretizing the Independent Variables (r, θ)

4.1.1 Discretizing the Azimuth θ

Given a radius $r > 0$ and an even number $N > 0$, we denote by

$$\{ (r, \theta_l) \mid \theta_l = \frac{2l\pi}{N} \} \tag{158}$$

the equispaced points on the circle $\{ (r, \theta) \mid \theta \in [0, 2\pi] \}$ (the value of N will be specified later in this subsection), so that functions on the circle are represented by their values at these points. In particular, the scatterer q and its perturbation δq on the circle are understood as real valued vectors of dimension N; the linear diagonal operator q_r (see Remark 2.8) is now a diagonal matrix of dimension N; the Fourier transform F and its inverse F^{-1} are understood as the discrete Fourier transforms (DFT) of dimension N; and the linear operator

$$\hat{q}_r = F \cdot q_r \cdot F^{-1} \tag{159}$$

(see (32)) is regarded as a matrix of dimension N. A sequence $\alpha = \{\alpha_m\} \in X_{kr}$ is truncated and rearranged in the DFT order

$$\{ \alpha_0, \alpha_1, \ldots, \alpha_{N/2}, \alpha_{-N/2+1}, \ldots, \alpha_{-1} \}; \tag{160}$$

so truncated and rearranged are the vectors in Y_{kr}, the matrices J_{kr}, H_{kr} and $S_{r,k}$. We will refer to the central entries of the vector (160) as the high-frequency entries. The high-frequency entries of the scattering matrix are those in the center rows and columns. A vector

$$\{ \beta_0, \beta_1, \ldots, \beta_{M/2}, \beta_{-M/2+1}, \ldots, \beta_{-1} \} \tag{161}$$

of dimension $M < N$ (M even) can be added to α by firstly zero padding β

$$\{ \beta_0, \beta_1, \ldots, \beta_{M/2}, 0, \ldots 0, \beta_{-M/2+1}, \ldots, \beta_{-1} \}, \tag{162}$$

and then carrying out the regular addition of two vectors of the same size. Similarly, a scattering matrix of dimension M can be viewed as of dimension N by zero padding.

Remark 4.1 *When matrices of different dimensions appear in an arithmetic operation (see, for example, (186)), the smaller matrices are first zero padded to the maximum dimension; the final result is a matrix of the maximum dimension.*

In the rest of this paper, we denote by $n_\theta(r) = N$. Numerical experiments show that $n_\theta(r)$ can be chosen between $2rk$ and $3rk$, which is to say, 2 to 3 points per wavelength along the arclength of the circle $|x| = r$. In our numerical experiments,

$$n_\theta(r) \geq 2.8rk. \tag{163}$$

4.1.2 Discretizing the Radius r

Over the interval $[0, \varpi]$, we employ two sets of equispaced computational grids:

$$\{ r_j = j \cdot h_r, \quad j = 0, 1, \ldots, n_r, \quad h_r = \frac{\varpi}{n_r} \}, \tag{164}$$

$$\{ \rho_m = m \cdot h_\rho, \quad m = 0, 1, \ldots, n_\rho, \quad h_\rho = \frac{\varpi}{n_\rho} \}, \tag{165}$$

with integers $n_r > n_\rho$. The first set of grid is used for the solution of initial value problem (146) and (147). The second set is for discretization of the integral in equation (156). Our experiments show that, with the second order ODE solver of Section 4.2,

$$n_r \sim 10 \frac{k\varpi}{\pi}, \tag{166}$$

namely, the grid is about ten points per wavelength over the interval $[0, \varpi]$. For convenience in computation, the ratio n_r/n_ρ is chosen as an integer, so that

$$\{ \rho_m \} \subset \{ r_j \}. \tag{167}$$

The ratio is 2 or 3 in our numerical experiments.

4.2 Solving the Forward Scattering Problem

The initial value problem (146) and (147) of the Riccati equation is solved by an second order, implicit, alternating scheme. Assuming that j is the step counter, we initially set $j = 0$, $r = 0$, and

$$\check{S}_{0,k} = 0. \tag{168}$$

For $j = 1, 2, \ldots, n_r$, $\check{S}$ is updated from r_{j-1} to r_j by the following procedures (with $\tau = (r_j + r_{j-1})/2$): if j is odd,

$$\check{S}_{r_j,k} - \check{S}_{r_{j-1},k} = h_r \frac{i\pi\tau}{2} k^2 (J_{kr_{j-1}} + \check{S}_{r_{j-1},k} \cdot H_{kr_{j-1}}) \times$$
$$\widehat{(q_{\bar{k}})}_\tau \cdot (J_{kr_j} + H_{kr_j} \cdot \check{S}_{r_j,k}); \tag{169}$$

29

if j is even,

$$\check{S}_{r_j,k} - \check{S}_{r_{j-1},k} = h_r \frac{i\pi\tau}{2} k^2 (J_{kr_j} + \check{S}_{r_j,k} \cdot H_{kr_j}) \times$$
$$\widehat{(q_{\bar{k}})}_\tau \cdot (J_{kr_{j-1}} + H_{kr_{j-1}} \cdot \check{S}_{r_{j-1},k}). \tag{170}$$

For each r_j, it requires $O\left(N_\theta^3(r_j)\right)$ operations to solve each of the linear systems (169), (170). Since there are n_r steps over $[0, \varpi]$ in the ODE solve, and since n_r, n_θ are both proportional to N_w (see (163), (166), and Remark 2.1), the total cost for solving the Riccati equation is $O(N_w^4)$.

4.3   Evaluating the Operators E_L, E_R

In this subsection, we discretize the linear equation (156) and evaluate E_L, E_R on the grid $\{\rho_m\}$. There are several ways to evaluate the matrices E_L, E_R; here, we present one of them. For convenience discussion, we first scale the linear system (156) using formulae (103), (104): multiplying (156) from the left by $E_L(\varpi, 0; P_y)$, and from the right by $E_R(\varpi, 0; P_x)$, we obtain

$$\frac{i\pi}{2} k^2 \int_0^\varpi E_L(r, 0; P_y) \cdot (J_{kr} + \check{S}_{r,k} \cdot H_{kr}) \cdot \widehat{(\delta q)}_r \times$$
$$(H_{kr} \cdot \check{S}_{r,k} + J_{kr}) \cdot E_R(r, 0; P_x) \cdot r \cdot dr$$
$$= E_L(\varpi, 0; P_y) \cdot (\delta S)_{\varpi,k} \cdot E_R(\varpi, 0; P_x). \tag{171}$$

The integration over $[0, \varpi]$ in (156) is discretized using the trapezoidal rule on the equispaced grids $\{\rho_m\}$:

$$\frac{i\pi}{2} k^2 h_\rho \sum_{j=0}^{n_\rho} \tilde{\rho}_j E_L(\rho_j, 0; P_y) \cdot (J_{k\rho_j} + \check{S}_{\rho_j,k} \cdot H_{k\rho_j}) \times$$
$$\widehat{(\delta q)}_{\rho_j} \cdot (H_{k\rho_j} \cdot \check{S}_{\rho_j,k} + J_{k\rho_j}) \cdot E_R(\rho_j, 0; P_x)$$
$$= E_L(\varpi, 0; P_y) \cdot (\delta S)_{\varpi,k} \cdot E_R(\varpi, 0; P_x). \tag{172}$$

where $\tilde{\rho}_j$ is defined as

$$\tilde{\rho}_j = \begin{cases} \rho_j & j = 1, 2, \ldots, n_\rho - 1, \\ \rho_j/2 & j = 0, n_\rho . \end{cases} \tag{173}$$

Although the two matrices $E_L(r, 0; P_y)$, $E_R(r, 0; P_x)$ are required at the coarser grid $r = \rho_m$, they will be first obtained on the finer grid $r = r_j$ in order to maintain an accuracy comparable to that in which the scattering matrix $\check{S}$ is obtained. We use formulae (110), (111) to recursively compute $E_L(r, 0; P_y)$, $E_R(r, 0; P_x)$ at $r = r_j$, $j = 1, 2, \ldots$. The recursion starts with the initial values

$$E_L(0, 0; P_y) = I, \tag{174}$$
$$E_R(0, 0; P_x) = I. \tag{175}$$

For $j = 1, 2, \ldots, n_r$, the matrix $E_L(r_j, 0; P_y)$ is updated from $E_L(r_{j-1}, 0; P_y)$ via the formula

$$E_L(r_j, 0; P_y) = E_L(r_{j-1}, 0; P_y)\left(I - \frac{h_r}{2}P_y(r_{j-1})\right)\left(I + \frac{h_r}{2}P_y(r_j)\right)^{-1}; \quad (176)$$

the matrix $E_R(r_j, 0; P_x)$ is updated from $E_R(r_{j-1}, 0; P_x)$ via the formula

$$E_R(r_j, 0; P_x) = \left(I + \frac{h_r}{2}P_x(r_j)\right)^{-1}\left(I - \frac{h_r}{2}P_x(r_{j-1})\right)E_R(r_{j-1}, 0; P_x). \quad (177)$$

4.4 Forming the Linear Equations

After $E_L(r_j, 0; P_y)$, $E_R(r_j, 0; P_x)$ are evaluated (see Section 4.3), and $\check{S}_{r_j,k}$ obtained from the forward solve (see Section 4.2), we write explicitly the linear equations (172) in terms of these matrices, so that we can see more clearly the structures of (172).

For $j = 1, 2, \ldots, n_\rho$, we denote by (see Section 4.1.1)

$$N_j = n_\theta(\rho_j) \quad (178)$$

the number of equispaced points on the circle $r = \rho_j$, which is also the dimension of the matrices $\check{S}_{\rho_j,k}$, $E_L(\rho_j, 0; P_y)$, and $E_R(\rho_j, 0; P_x)$. Given j and for $0 \leq m < N_j$, we further denote by

$$\theta_{j,m} = \frac{2m\pi}{N_j} \quad (179)$$

the azimuthal values of the equispaced points on the circle $r = \rho_j$. Finally, for a smooth function g, we denote by $g_{j,m}$ the values of g at the equispaced points on the circle. We will require the matrix of dimension N_{n_ρ}

$$dS = (\delta S)_{\varpi,k}, \quad (180)$$

and the three matrices of dimension N_j

$$B_j = E_L(\rho_j, 0; P_y)\cdot(J_{k\rho_j} + \check{S}_{\rho_j,k}H_{k\rho_j})\cdot(N_j^{\frac{1}{2}}F), \quad (181)$$

$$A_j = (N_j^{\frac{1}{2}}F^{-1})\cdot(J_{k\rho_j} + H_{k\rho_j}\check{S}_{\rho_j,k})\cdot E_R(\rho_j, 0; P_x), \quad (182)$$

$$(\delta q)_j = diag\{ (\delta q)_{j,0}, (\delta q)_{j,1}, \ldots, (\delta q)_{j,N_j} \}, \quad (183)$$

where $N_j^{\frac{1}{2}}F$ and $N_j^{\frac{1}{2}}F^{-1}$ are scaled discrete forward and backward Fourier transforms, so that

$$(N_j^{\frac{1}{2}}F)_{m,n} = \exp\left(-i\frac{2mn\pi}{N_j}\right), \quad (184)$$

$$(N_j^{\frac{1}{2}}F^{-1})_{m,n} = \exp\left(i\frac{2mn\pi}{N_j}\right). \quad (185)$$

31

Then, with the help of (181), (182), (183), (159), we rewrite the linear equation (172) in the form

$$\frac{i\pi}{2}k^2 h_\rho \cdot E_L(0,\varpi; P_y) \cdot \left(\sum_{j=0}^{n_\rho} \frac{\tilde{\rho}_j}{N_j} \cdot B_j \cdot (\delta q)_j \cdot A_j \right) \cdot E_R(0,\varpi; P_x) = dS, \qquad (186)$$

(with the summation of matrices of different dimensions discussed in Remark 4.1). Denoting by $\mathcal{D}$ the linear space of real-valued vectors of dimension

$$N_q = \sum_{j=1}^{n_\rho} N_j, \qquad (187)$$

and by $\mathcal{R}$ the linear space of complex-valued vectors of dimension

$$N_s = N_{n_\rho}^2, \qquad (188)$$

we observe that $dS \in \mathcal{R}$, that (186) is a system of linear equations for the vector $\delta q \in \mathcal{D}$ defined by

$$\begin{aligned} \delta q = \quad \{ \quad &((\delta q)_{1,0}, (\delta q)_{1,1}, \ldots, (\delta q)_{1,N_1-1}), \\ &((\delta q)_{2,0}, (\delta q)_{2,1}, \ldots, (\delta q)_{2,N_2-1}), \\ &\ldots, \\ &((\delta q)_{n_\rho,0}, (\delta q)_{n_\rho,1}, \ldots, (\delta q)_{n_\rho,N_{n_\rho}-1}) \quad \}^T, \qquad (189) \end{aligned}$$

and that (186) defines a linear operator $\mathcal{A} : \mathcal{D} \mapsto \mathcal{R}$, such that (172) can be reformulated as

$$\mathcal{A}\,(\delta q) = dS. \qquad (190)$$

Remark 4.2 *It is easy to see that the procedures for obtaining the matrices $\{ A_j, B_j, j = 1, 2, \ldots, n_\rho \}$, as well as the application of $\mathcal{A}$ to a vector, cost $O(N_w^4)$ arithmetic operations.*

Remark 4.3 *We define the inner product in the range space $\mathcal{R}$ by the formula*

$$(u,v) = \sum_{j=1}^{N_s} u_j \cdot v_j \qquad (191)$$

so that the induced norm for $\mathcal{R}$ is the standard L^2 norm. Since vectors in $\mathcal{D}$ of the form (189) represent functions of $L^2(D(\varpi))$ in polar coordinates, and since the inner product of a pair of functions in $L^2(D(\varpi))$ defined by the formula

$$(f,g) = \int_0^\varpi \left(\frac{1}{2\pi} \int_0^{2\pi} \overline{f(r,\theta)} \cdot g(r,\theta) d\theta \right) \cdot r \cdot dr, \qquad (192)$$

32

induces the L^2 norm, we accordingly define the discrete version of (192) by the formula

$$(x, y)_r = h_\rho \sum_{j=0}^{n_\rho} \tilde{\rho}_j \left(\frac{1}{N_j} \sum_{m=0}^{N_j-1} \overline{x}_{j,m} y_{j,m} \right), \qquad (193)$$

as the inner product for the vectors x, $y \in \mathcal{D}$. We refer to the norm of $\mathcal{D}$ induced by (192) as the L^r norm.

4.5 Least-square Solution of the Linearized Equation

In order to solve the least-squares problem (190), the conjugate-gradient method was employed (to the normal equation of (190)) because it is the least expansive among several standard methods, including QR decomposation, Gram-Schmidt orthogonalization. The application of the conjugate-gradient method, in this case, is tedious and straightforward with one exception. The inner product (193) must be used (see Remark 4.3) to obtain the least-squares solution in $\mathcal{D}$, namely, the minimization of the solution in the L^r norm of $\mathcal{D}$, as well as the minimization of the residual in the L^2 norm of $\mathcal{R}$. More specifically, this means that the inner product in a standard conjugate-gradient method must be replaced with (193). It also means that the adjoint operator of $\mathcal{A}$ (see (190)) must be redefined as follows. We denote by A a matrix of dimension $N_s \times N_q$ whose i-th row, $a^{(i)}$, is such that

$$\left(\left[a^{(i)} \right]^*, \, y \right)_r = [\mathcal{A}(y)]_i \qquad (194)$$

for all $y \in \mathcal{D}$. Obviously, the Hermitian of A, namely, the linear operator $A^* : \mathcal{R} \mapsto \mathcal{D}$, is the adjoint operator of $\mathcal{A}$, with respect to the inner product (191) in $\mathcal{R}$, and to the inner product (193) in $\mathcal{D}$. Let $\delta q = A^* u$, where $u \in \mathcal{R}$ in the form of an $N_s \times N_s$ matrix, and δq in the form (189). It is a tedious but straightforward manipulation to show that

$$\overline{(\delta q)_{j,m}} = \frac{ik^2}{4} \sum_{n,l=1}^{N_j} \{A_j\}_{m,n} \cdot \{B_j\}_{l,m} \cdot \{ E_R(0, \varpi; P_x) \cdot u^* \cdot E_L(0, \varpi; P_y) \}_{n,l} \qquad (195)$$

where $\{T\}_{m,n}$ denotes the (m, n)-th entry of the matrix T.

Remark 4.4 *It is easy to see from (195) that the application of $\mathcal{A}^*$ to a vector cost $O(N_w^4)$ arithmetic operations (see also Remark 4.2).*

Remark 4.5 *Since only an approximate solution of the least-squares is required (see Remark 3.14), the conjugate-gradient iteration is usually terminated at n-th step in our numerical experiments when the ratio of norms of the last and the initial residuals*

$$\sigma = \frac{\|r_n\|}{\|r_0\|} \qquad (196)$$

is about 10^{-3}.

5   Numerical Results and Discussions

FORTRAN programs have been written implementing the procedures described in the preceding section. In this section, to illustrate the performance of the algorithm, we present several numerical examples for the inversion of the Helmholtz equation in two dimensions. Remarks will be made, at the beginning and the end of this section, to discuss some technical details of the numerical experiments.

5.1   The Up-recursion and the Complexity

In our numerical implementations, only an approximate q_{k_1} is sought to start the recursive procedure described in Section 3.6). We find consistently in our numerical experiments that the lowest frequency k_1 can be chosen such that its corresponding wavelength is the about size of the scatterer.

Remark 5.1 *Our numerical experiments further show that frequently k_j (see Figure 7) can be chosen such that the size of the scatterer is about j wavelengths. For instance, we may set*

$$k_j = j, \tag{197}$$

for a scatterer, whose function q is not large, inside a disk of diameter 2π.

Assuming a finite number of iterations are required in the conjugate gradient method, for the linear system (157) needs not be solved accurately according to Remark 3.14, we observe that the least-squares solution of (157) can be approximately obtained at a cost of $O(N_w^4)$ arithmetic operations (see Remarks 4.2, 4.4). Then, the inversion algorithm requires $O(N_w^5)$ operations since there are about N_w frequencies employed in the recursion (see Remark 5.1).

5.2   The Forward Modeling

The scattering data (see Section 2.2) are obtained by numerical solution of the forward scattering problem—the initial value problem of the Riccati equations (see (34) and (26)). In our numerical computation, we assume the scatterer q is nonzero in a disk of radius $\varpi = \pi$.

We used both the standard fourth order Runge-Kutta method and the second order implicit scheme described in Section 4.2 for the numerical solution of the ordinary differential equation (34). The numerically obtained solutions were compared with the exact ones when they were analytically available. We found that both methods converged at rates as expected, with the former being more efficient if the accuracy required was higher that 10^{-4}. For general scatterers to which exact solutions of the scattering matrix were not available, the rates of convergence of the two methods were verified numerically. In the numerical

reconstructions presented below, the scattering data used were all obtained with an accuracy 10^{-3} to 10^{-4}.

5.3 Numerical Examples

A large number of numerical experiments have heen made in which several types of the scatterers have been reconstructed. The reconstructions of five types of scatterers are presented here. The biggest problems that have been tested are about forty wavelengths, which require two to three hours CPU time on a c-90 Cray computer.

Example 1: Reconstruct a scatterer defined by

$$q_1(x,y) = 0.15 \cdot (1-x)^2 \cdot e^{-(x^2+(y+1)^2)} - 0.5 \cdot \left(\frac{x}{5} - x^3 - y^5\right) \cdot e^{-(x^2+y^2)}$$
$$- \frac{1}{60} \cdot e^{-((x+1)^2-y^2)}, \tag{198}$$

inside the disk $D(\pi)$; see Figure 8 for surface and contour plots of the scatterer function. Nine frequencies were used in the reconstruction, corresponding to wave numbers $k = 1, 2, \cdots, 9$. The inversion algorithm reconstructed it accurately (the

k	1	2	3	4	5	6	7	8	9
e_2	0.57	0.41	0.16	3.1-2	6.4E-3	2.2E-3	1.2E-3	7.9E-4	5.6E-4

Table 1: L^2 Error of Reconstruction at 9 Frequencies, Example 1.

reconstructed function will not be plotted against the exact since the error is so small that it is invisible in the plot). The procedure cost 122 seconds CPU time on a Cray C-90 computer; see Table 1 for the L^2 error of the reconstruction.

Example 1.1: To test the stability of the algorithm, we reconstruct in this example the scatterer q_1 but with noisy data. Noise is added to the scattering data used in Example 1 by truncating each number in the data to certain digits. For instance, truncating the number 0.129876 to two digits yields 0.12, and the perturbation (or noise) incurred here by the truncation is about 1%. Three tests were made here corresponding to truncations of the scattering data to $N_d = 3, 2, 1$ digits. The resulting errors in the inversion are listed in Table 2.

N_d	3	2	1
e_2	1.4E-3	1.3E-2	1.1E-1

Table 2: L^2 Error of Reconstruction with Noisy Data, Example 1.1.

Figure 9 shows the surface and contour plots of the reconstruction with the scattering data truncated to one digit, namely, the noisy data used here only have one-digit accuracy. This is a quite severe test to an algorithm. This time, not only our computation didn't blow up, it actually reconstructed the scatterer with a 11% error. Stability tests were also performed to other scatterers whose reconstructions are presented in this paper, the results being similar.

Example 2: Reconstruct a scatterer defined by

$$q_2(x,y) = 0.2\left\{1 + \cos(11 \cdot x) + \sin(11 \cdot y)\right\}, \tag{199}$$

inside $D(\pi)$; see Figure 10 for surface and contour plots of the scatterer. This is a quite oscillatory function. Inside the disk, there are about 160 peaks and valleys representing a highly rugged index of refraction. The computation simulates an acoustic experiment in which the background speed of sound is that of water; the scatterer is 20.87 centimeters in diameter (about the size of a human head). Nine frequencies, $f = 7, 14, 21, \cdots, 63$ kHz, were used in the reconstruction, corresponding to wave numbers $k = 1, 2, \cdots, 9$. At $f = 63$ kHz, 108 transducers were required around the scatterer. The procedure cost 122 seconds CPU time on a Cray C-90 computer; see Table 3 for the L^2 error of the reconstruction.

k	1	2	3	4	5	6	7	8	9
e_2	0.53	0.56	0.56	0.55	0.25	8.2E-2	3.6E-2	1.9E-2	1.2E-2

Table 3: L^2 Error of Reconstruction at 9 Frequencies, Example 2.

Because of the complicated structure of the scatterer, the reconstructed scatterer is plotted against the exact scatterer first horizontally across the diameter of the disk $D(\pi)$, then across concentric circles of various radii between 0 and π of the disk; see Figures 11, 12.

Example 3: Reconstruct a scatterer defined in $D(\pi)$ by

$$q_3(x,y) = \begin{cases} q_1(x/0.8, y/0.8) & \text{if } r < 2.6, \\ -0.5 & \text{if } r \in [2.6, 2.9), \\ 0 & \text{if } r \geq 2.9; \end{cases} \tag{200}$$

see Figure 13 for surface and contour plots of the function. This scatterer is difficult to reconstruct for two reasons.

(1) Across the two circles $r = 2.6$ and $r = 2.9$, the function is discontinuous. The value of the function changes sharply to -0.5 in the narrow annulus.

(2) If the background speed of sound is that of water, then the material in the narrow band $2.6 \leq r \leq 2.9$ has speed of sound 1.4 times as large as that of water. As a result, this high-speed region with sharp boundaries blocks the passage of the probing sound waves to the inside of the structure, making it hard to reconstruct the smooth part of the scatterer in the middle of the object.

This example could be regarded as a model problem for ultrasound tomography of a human head, where the skull is represented by the thin layer of denser material in the region $2.6 \leq r \leq 2.9$. If the actual object is 20.87 centimeters in diameter, the frequencies used were $f = 7, 14, 21, \cdots, 84$ kHz, corresponding to wave numbers $k = 1, 2, \cdots, 12$. At $f = 84$ kHz, 128 transducers were used around the scatterer. The CPU time required for the procedure was 263 seconds on a Cray C-90 computer. The L^2 errors of the reconstruction at the 12 frequencies

k	1	2	3	4	5	6
e_2	0.576	0.510	0.367	0.260	0.231	0.220
k	7	8	9	10	11	12
e_2	0.197	0.164	0.146	0.141	0.138	0.136

Table 4: L^2 Error of Reconstruction at 12 Frequencies, Example 3.

are listed in Table 3. Figure 14 shows the surface and contour plots of the reconstructed scatterer, whereas Figure 15 shows the reconstruction horizontally across the diameter of the scatterer.

An examination of the plots show that the error of the reconstructions occurs largely around the discontinuities, while the smooth part is recovered more accurately.

Example 4: Reconstruct a cylindrically symmetric scatterer defined by

$$q_4(r) = 0.3 \cdot [\, 0.55 \cos(2r) - 0.44 \sin(4r) + 0.23 \sin(6r) + 0.3 \cos(8r) \,], \quad (201)$$

for $0 \leq r \leq \pi$. Nine frequencies were used in the reconstruction, corresponding to wave numbers $k = 1, 2, 3, \cdots, 9$. The purpose of this example is to show how the Uncertainty Principle works by illustrating the process of convergence and the distributions of error in reconstructions at these nine frequencies. An examination of the plots of the reconstructions and error functions shows that

(1) The largest error of the reconstructions occurs near the two points $r = 0$, $r = \pi$ where the scatterer is not smooth.

(2) The error function $q - q_k$ is more or less evenly distributed away from the end points $r = 0$, $r = \pi$.

37

(3) The higher the wave number k is, the more oscillatory the error function becomes.

Example 5: Reconstruct a cylindrically symmetric scatterer in the disk $D(\pi)$ defined as follows. Give $r_0 > 0$, the scatterer function is given by the formula

$$q_5(r) = 0.4 \cdot \left[1 - \cos \left(6 \cdot \frac{r - r_0}{\pi - r_0} \right) \right], \tag{202}$$

for $r_0 \leq r \leq \pi$. Inside the disk $D(r_0)$, the scatterer function q is not defined; on the circle $r = r_0$, the Dirichlet boundary condition is imposed on the total field ϕ. Therefore, the circle $|x| = r_0$ is a totally reflecting surface, and the medium inside $D(r_0)$ is "sound-soft" (see, for example, [1], page 319–321 for the treatment of exterior Dirichlet problem). We choose $r_0 = 0.8$ in the numerical computation. Fifteen frequencies were used in the reconstruction, corresponding to wave numbers $k = 1, 2, 3, \cdots, 12$.

The inversion algorithm doesn't know the fact that part of the scattering is due to a reflecting surface. Rather, it assumes that the scattering occurs as a result of a distribution of an unknow index of refraction everywhere continuous: on the disk $D(\pi)$, across the circle $r = r_0$, and inside the disk $D(r_0)$. The purpose of this example is to see whether the inversion algorithm will be stable and convergent, and, if so, what this reconstructed continuous function q will be, particularly across the reflecting surface and inside the disk $D(r_0)$.

Our numerical experiments show that the reconstruction is indeed stable and convergent, see Figure 18 for the plots of the reconstructed q_k depicted against the exact q at the fifteen frequencies. In the pictures, the exact q is set zero in the interval $[0, r_0]$ to indicate that it is not defined inside $D(r_0)$. The L^2 errors given in Figure 18 are measured in the interval $[r_0, \pi]$. Two comments can be made about the reconstruction:

(1) Inside the totally reflecting disk, there are regions where the values of the reconstructed q_k are less than -1. After the reconstruction starts to converge, namely, when k is greater than 4, $q_k(r)$ decreases as r moves across the reflecting disk, and becomes less than -1 the moment r moves into the reflecting circle $r = r_0$. In other words, the inversion algorithm sees the reflecting disk as a region where the speed of sound of the medium is imaginary according to the formula

$$k\sqrt{1 + q(r)} = \frac{\omega}{c(r)}, \tag{203}$$

where $\omega > 0$ is the angular frequency, $c(r) > 0$ is the speed of sound. Therefore, to the full aperture experiment where the scattering data are collected, a reflecting disk looks the same (see Definition 3.8) as a layer of non-propagating medium.

(2) Outside the totally reflecting disk, the smooth part of the prescribed scatterer is essentially recovered: the reflecting surface is regarded as a discontinuity

38

of some type, which causes the Gibbs phenomenon around it; the scatterer function (202) is reconstructed more accurately away from this singular point.

5.4 Discussions and Conclusions

The following technical details of the numerical implementation appear to be worthy mentioning.

1. The convergence of recursive linearization procedure depends, of course, on the step size of the frequency k. We find in our numerical experiments that when the scatterer function is not large (for example, when $-0.8 \leq q \leq 1$), convergence is usually guaranteed with the step size given by (197). In general, smaller step sizes are required when the scatterer function is very large or very closed to -1. On the other hand, larger step sizes of k can generally be used at higher frequencies k without affecting the convergence. This is so because at a relatively high frequency $k = a$ where the dominant lower-frequency components of the scatterer have been recovered, $q - q_a$ is small. Therefore, the perturbation $\delta q = q_b - q_a$ will be small for a relatively large step size of $\delta k = b - a$.

2. The stability of the algorithm is not sensitive to the step size of the frequency k. It is largely controlled by the way the ill-posed linear system (157) is solved. Numerical experiments show that the up-recursion in frequency k is usually unstable when the least-squares solution of (157) is obtained in such a precision that σ (see (196)) is smaller than 10^{-6}. With scattering data accurate to three digits, we find that $\sigma = 10^{-3}$ (see Remark 4.5) is suitable to inversion in a varieties of cases.

The following discussions are about the models of forward scattering.

3. The use of cylindrical geometry to introduce the scattering matrix, and subsequently, to obtain the Riccati equation, is a convenient but not the only approach to the forward modeling. Scattering matrix associated with straight-line geometry, and its Riccati equation, for example, are introduced in [10].

4. Forward models other than the Riccati equations can be used to recursively linearize the inverse problem. The Lippmann-Schwinger equation seems a better candidate for the forward modeling because there is a recursive procedure that solves accurately the forward problem in $O(N_w^3)$ operations at a frequency. Thus, the multi-frequency inversion costs about $O(N_w^4)$ operations. The linearization procedure based on the Lippmann-Schwinger equation is described in [12]. Its implementation and numerical results will be reported on a later date.

The following discussions are about extentions of the algorithm to three dimensions and to other types of scattering problems.

5. The direct extention of the recursive linearization procedure to three dimensions is straightforward, but is difficult to be implemented numerically, for the procedure requires $O(N_w^8)$ operations. The high computational cost in three dimensions is primarily a result of the so-called data redundancy: at a frequency $k > 0$, the full-aperture scattering data depend on four independent parameters whereas the scatterer q to be recovered is a function of three spatial parameters. There are several ways to reduce the cost to $O(N_w^6)$; each of which uses part of the full-aperture scattering data.

6. The recursive procedure can be applied to measurements of limited aperture (see [12] for more details). In two dimensions, this only allows us to recover partial information of the scatterer within the Fourier aperture $D(2k)^+$. In three dimensions, measurements of limited aperture may provide the same amount of information about the scatterer as do the full-aperture measurements.

7. The scheme can be used to solve inverse scattering problems of more complicated equations describing more realistic processes of acoustic, elastic, or electromagnetic scattering in which the Heisenberg's Uncertainty Principle holds. The exact formulation of the uncertainty principle may differ in specific environments, but it is certain that everywhere in the realm of wave phenomena an incident wave of a lower frequency interacts weakly with the Fourier modes of the scatterer of higher frequencies, and such an interaction produces a weaker scattered field.

8. Heisenberg's Uncertainty Principle is also valid in the case of obstacle scattering. There, lower-frequency incident fields interacts weakly with the higher-frequency roughness of the surface of the scattering obstacle. Therefore, the inverse obstacle scattering problem can be recursively linearized by the same mechanism introduced here in this paper.

References

[1] Eyges, L. (1972), *The Classical Eletromagnetic Field,* Dover, New York.

[2] N. Bleistein (1984), *Mathematical Methods for Wave Phenomena,* Academic Press, New York.

[3] Abramowitz, M., and Stegun, I. (1965), *Handbook of Mathematical Functions,* Dover, New York.

[4] G. Matviyenko (1992), *On the Evaluation of Bessel Functions,* Research Report 903, Department of Computer Science, Yale University.

[5] G. N. Watson (1958), *A Treatise on the Theory of the Bessel functions,* Cambridge University Press, Cambridge.

[6] D. Colton and R. Kress (1983), *Inverse Acoustic and Electromagnetic Scattering Theory,* Wiley-Interscience Publication, New York.

[7] V. Rokhlin (1990), *Rapid Solution of Integral Equations of Scattering Theory in Two Dimensions,* Journal of Computational Physics, 86(2): 414

[8] G. Beylkin and R. Burridge (1990), *Linearized Inverse Scattering Problems in Acoustics and Elasticity,* Wave Motion 12 15–52.

[9] J. Sylvester (1992), *A Convergent Layer Stripping Algorithm for the Radially Symmetric Impedance Tomography Problem, Communications in PDE* **17**, No.12, pp.1955–1994.

[10] Y. Chen (1992), *On the Inverse Scattering Problem for the Helmholtz Equation in One Dimension,* Research Report 913, Department of Computer Science, Yale University.

[11] Y. Chen and V. Rokhlin (1995), *On the Riccati Equations for the Scattering Matrices in two dimensions,* Technical Report 1081, Department of Computer Science, Yale University.

[12] Y. Chen (1995), *Recursive Linearization for Inverse Scattering,* Technical Report 1088, Department of Computer Science, Yale University.
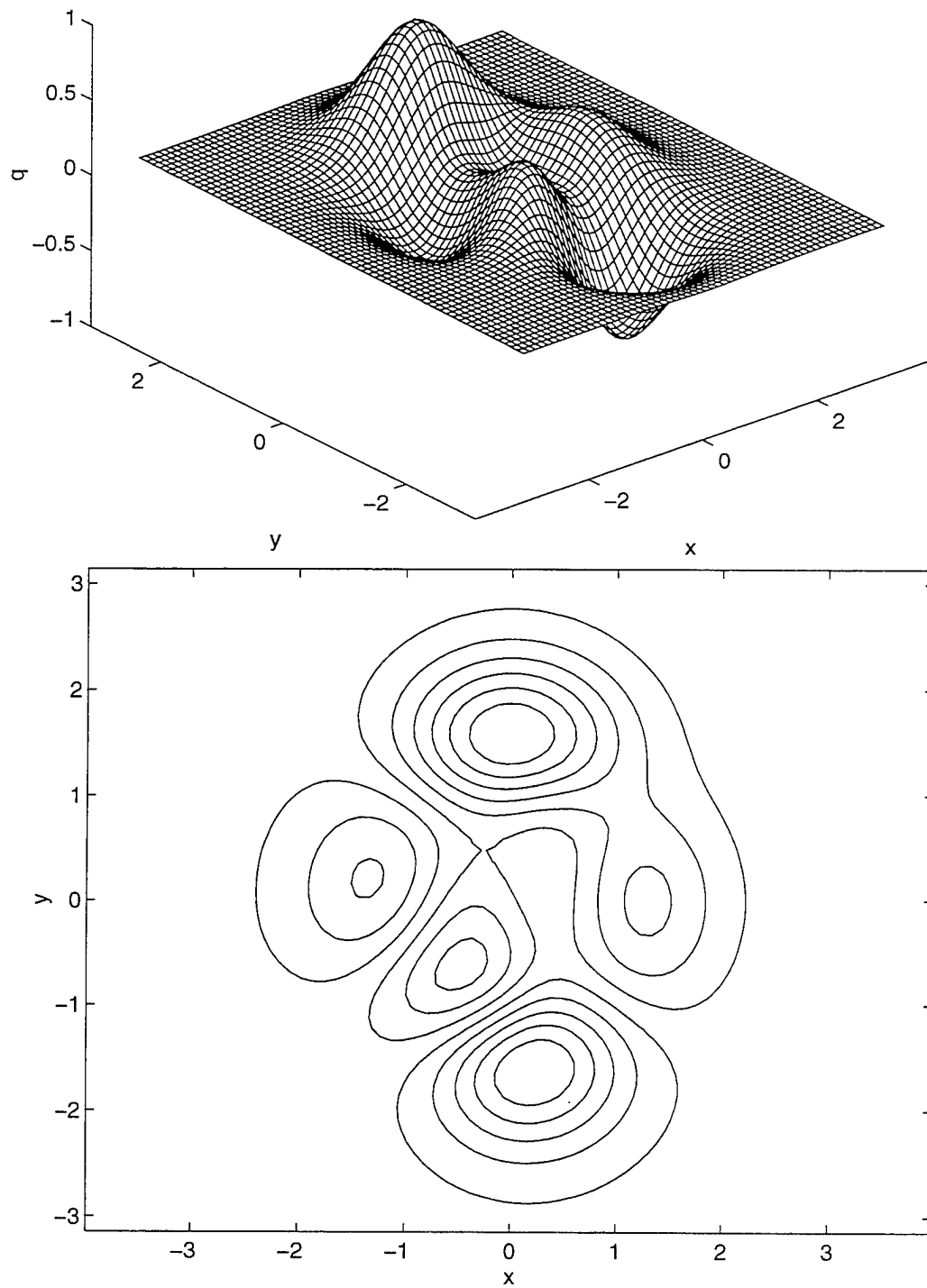
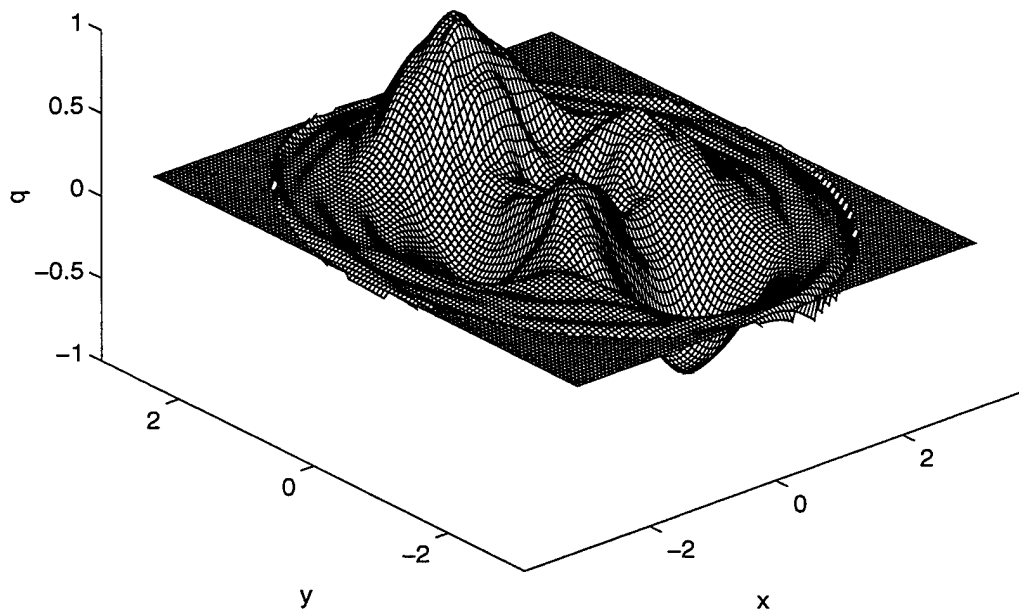Figure 8: Surface and Contour Views of Scatterer q_1, Example 1.
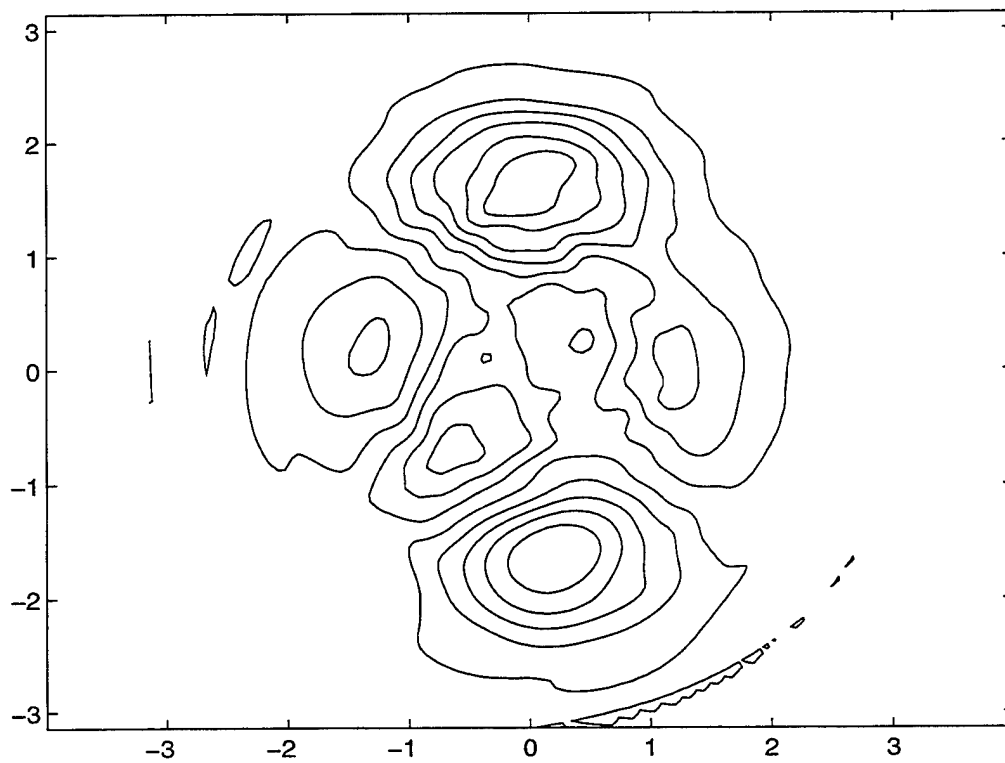
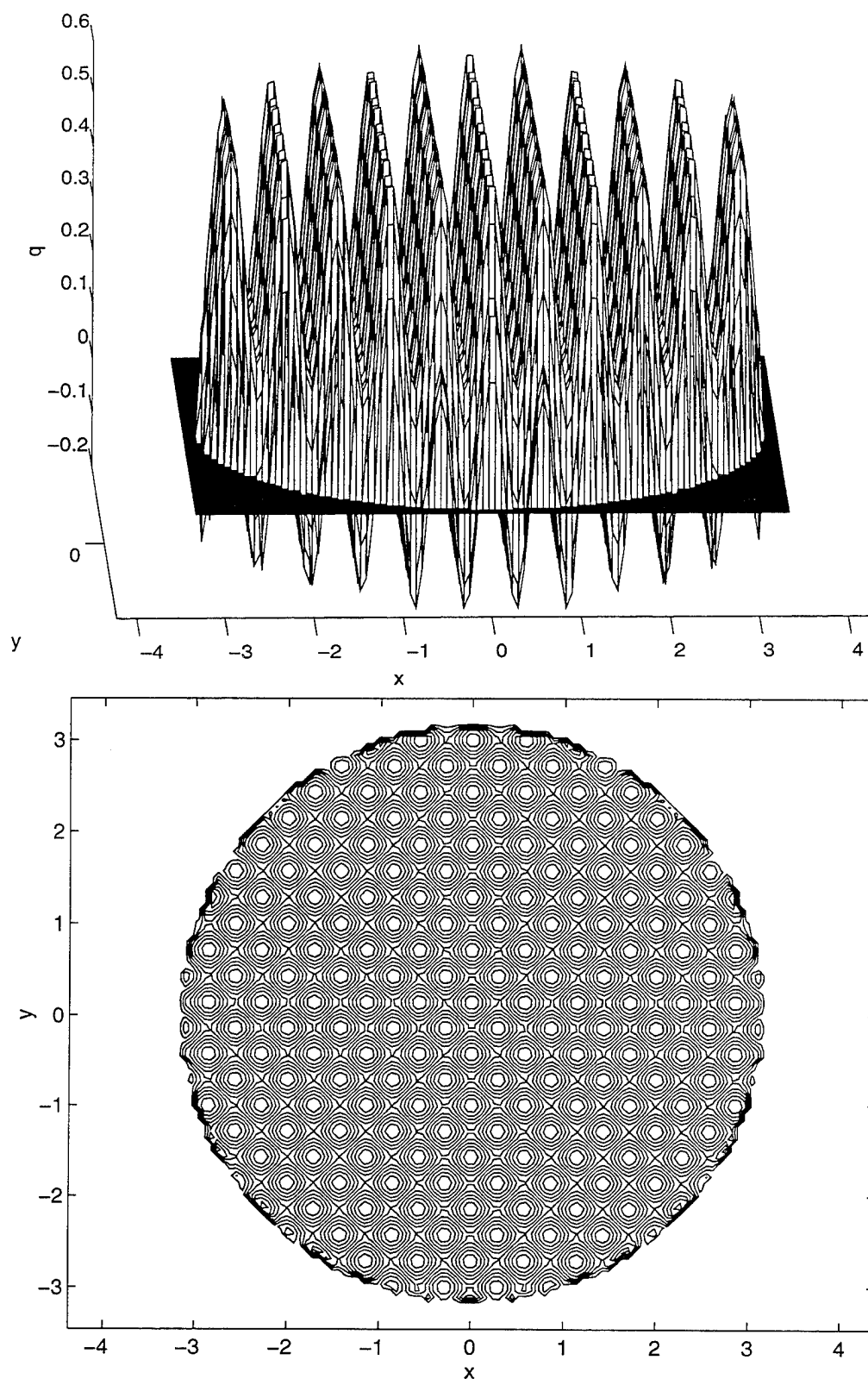Figure 9: Surface and Contour Views of Inversion with $N_d = 1$, Example 1.1.

Figure 10: Surface and Contour Views of Scatterer q_2, Example 2.

44
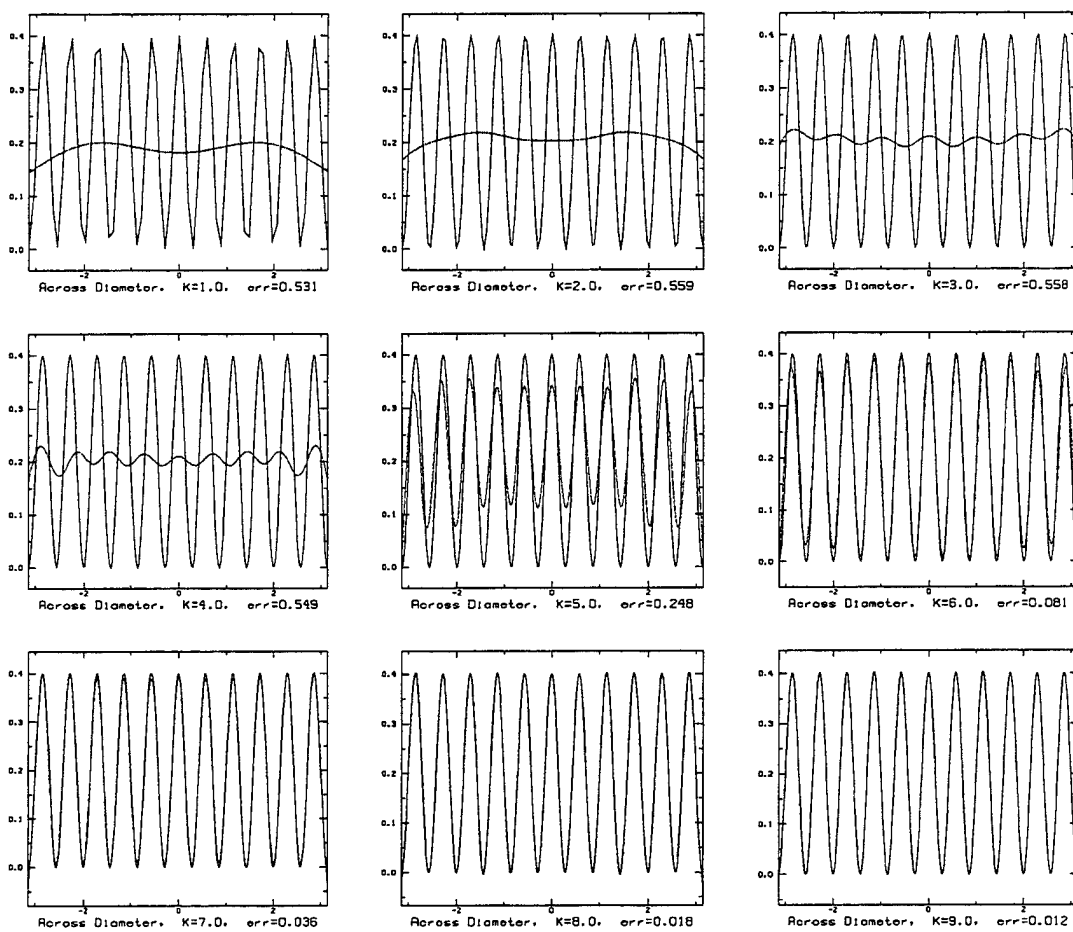
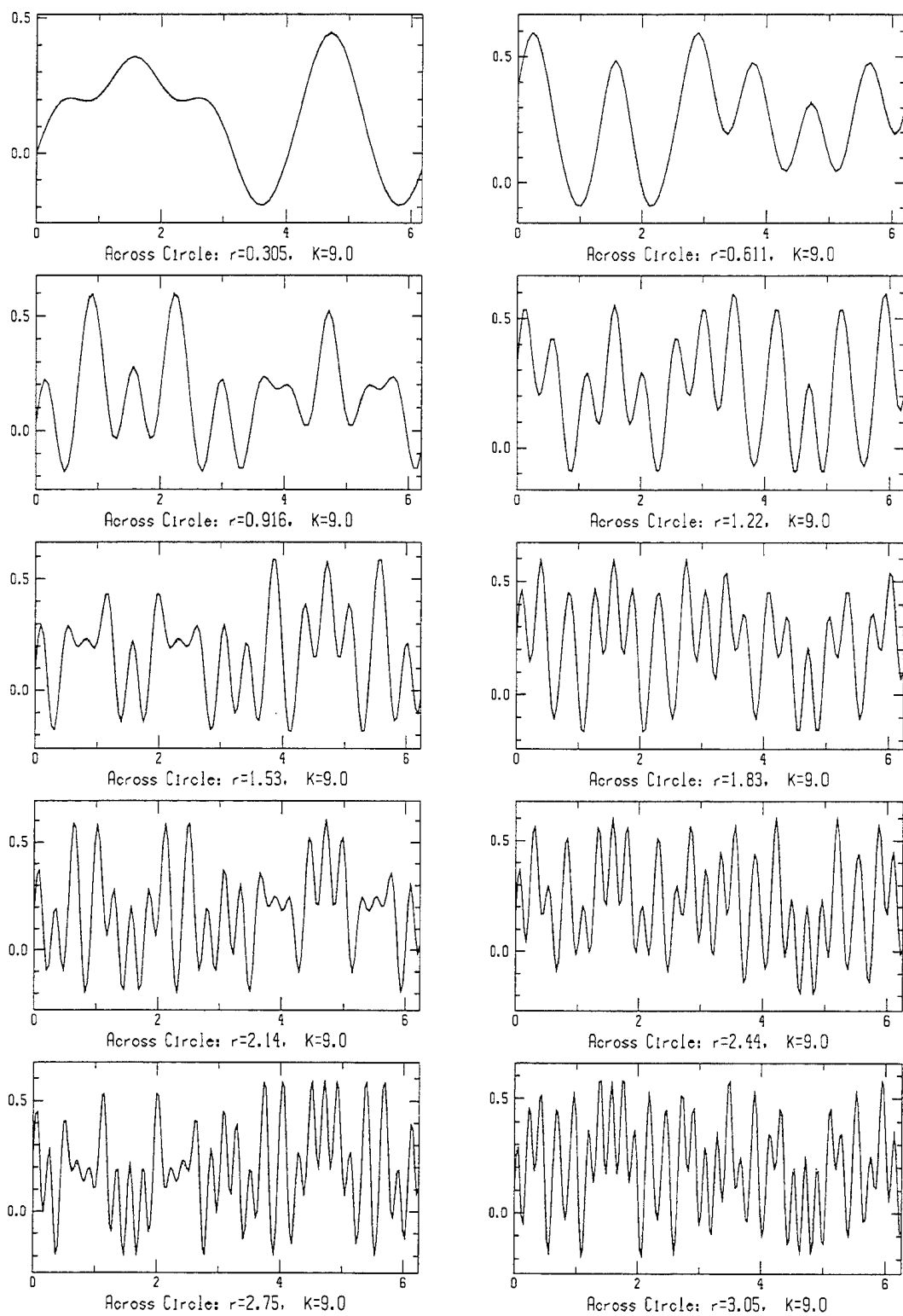Figure 11: Reconstructed vs Exact q_2 on Diameter, $k = 1, 2, \ldots 9$, Example 2.

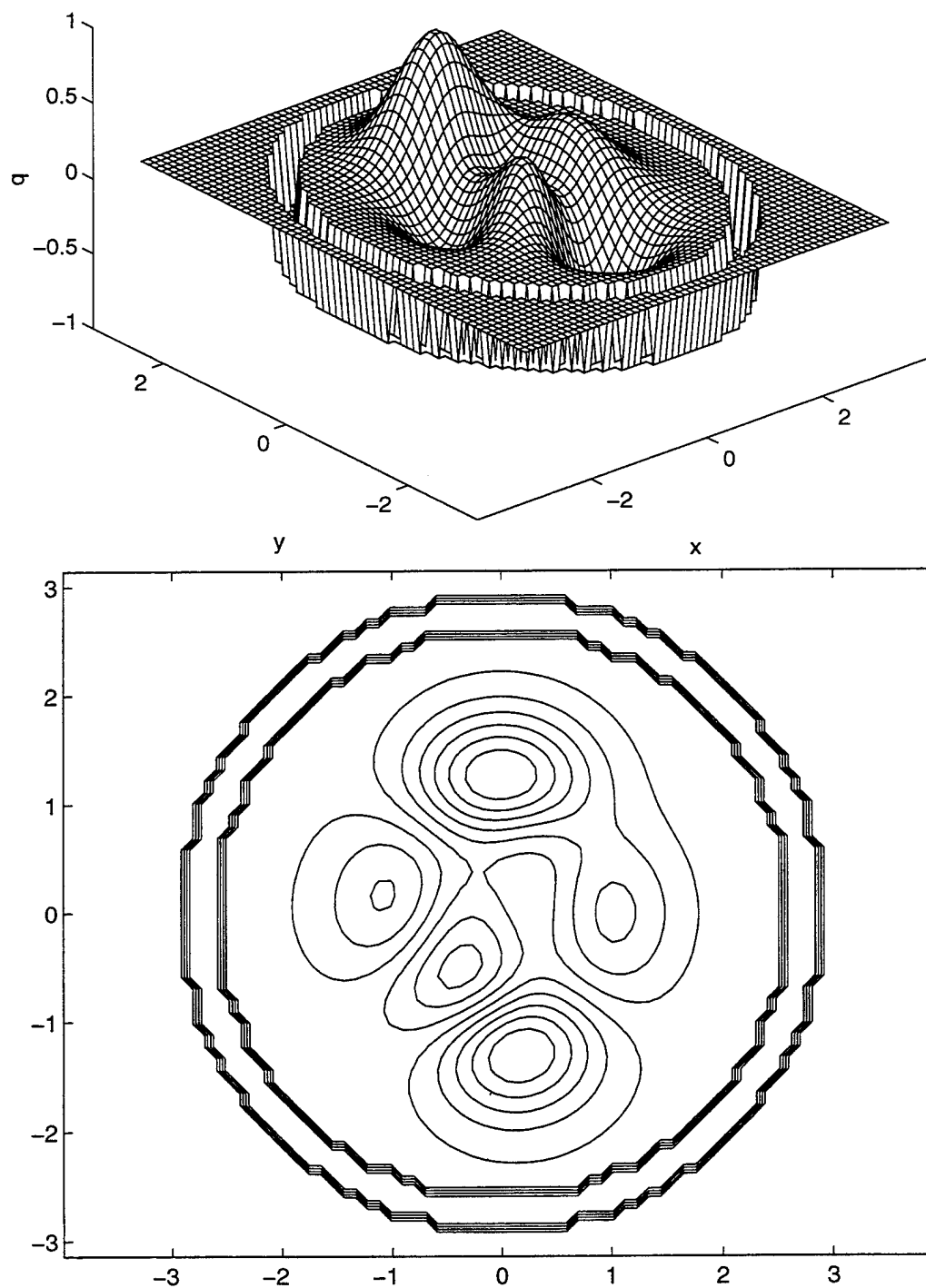Figure 12: Reconstructed vs Exact q_2 on Circles, $k = 9$, Example 2.

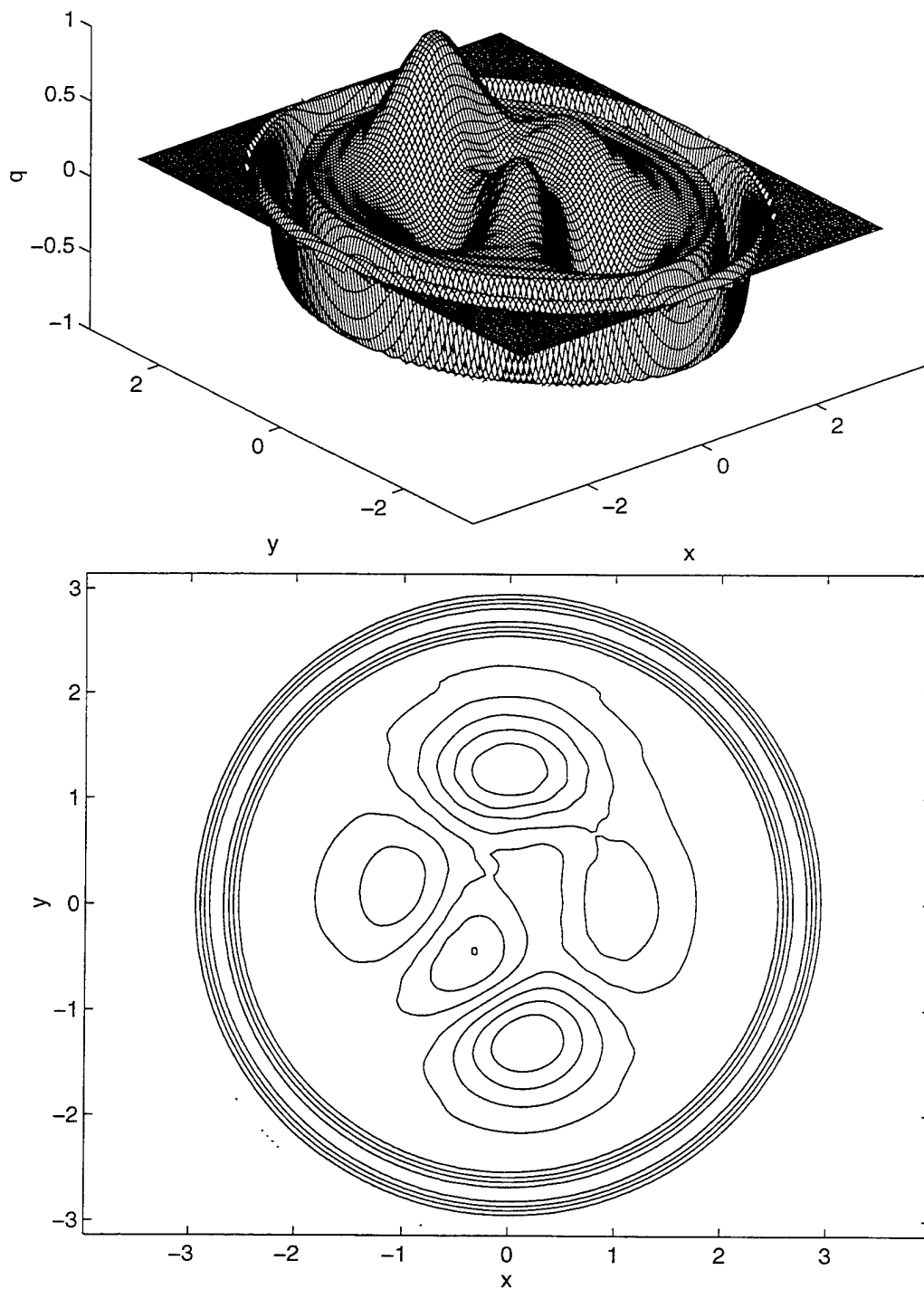Figure 13: Surface and Contour Views of Scatterer q_3, Example 3.

Figure 14: Surface and Contour Views of Reconstructed q_3, Example 3.
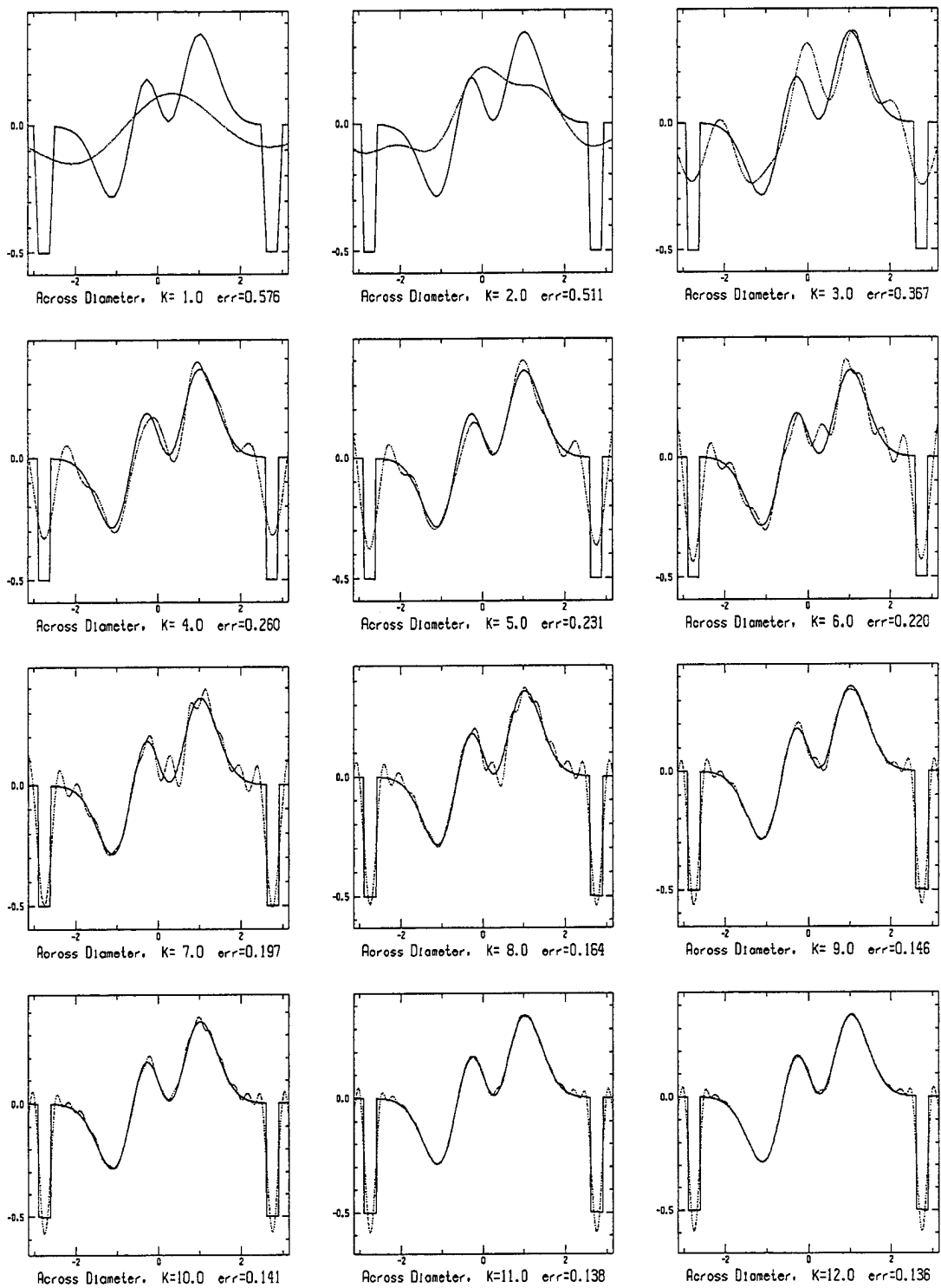
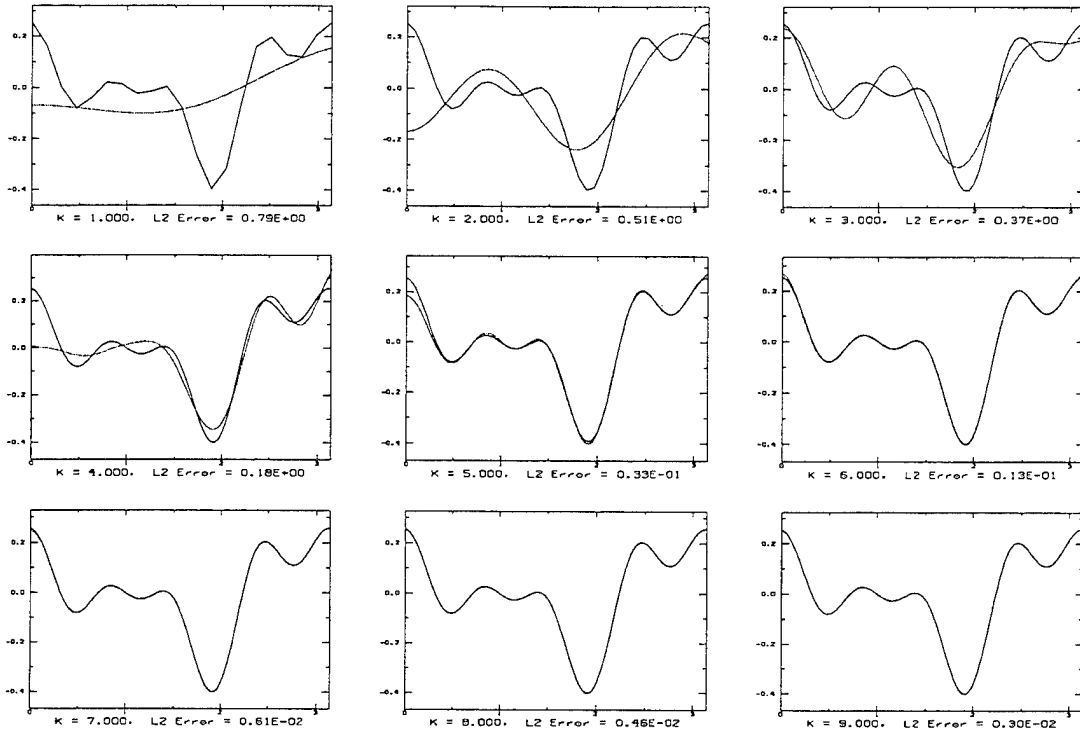Figure 15: Reconstructed vs Exact on Diameter at 12 Frequencies, Example 3.

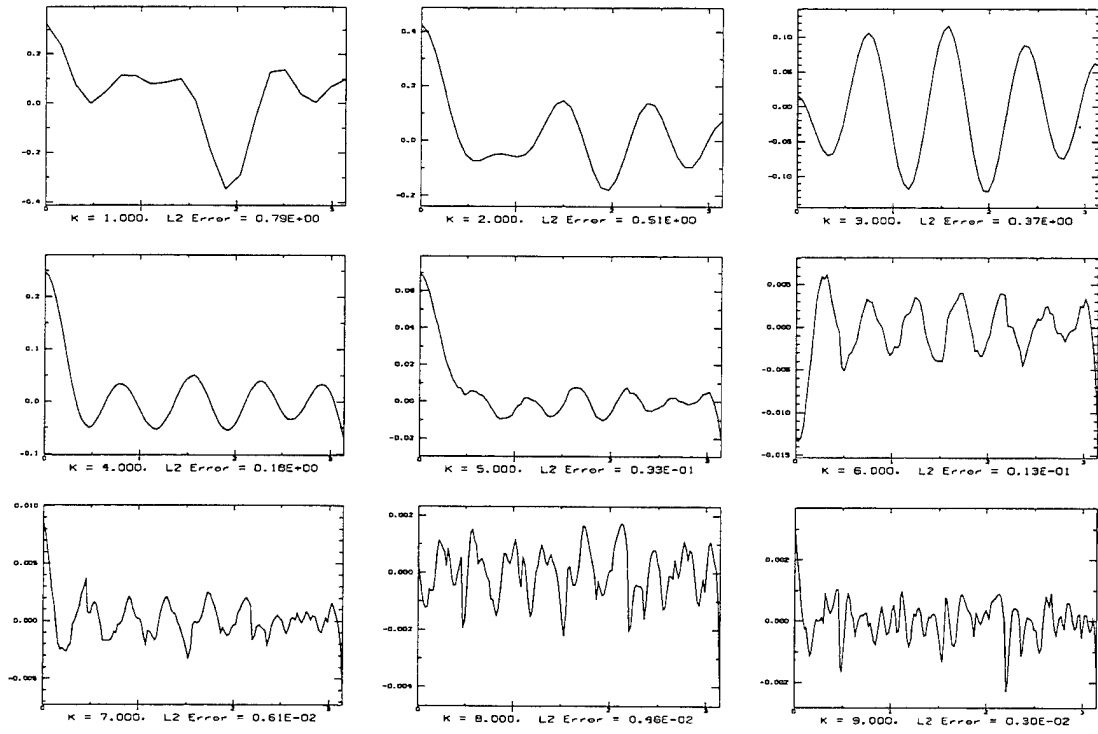Figure 16: Reconstructed vs Exact q_4 at 12 Frequencies, Example 4.

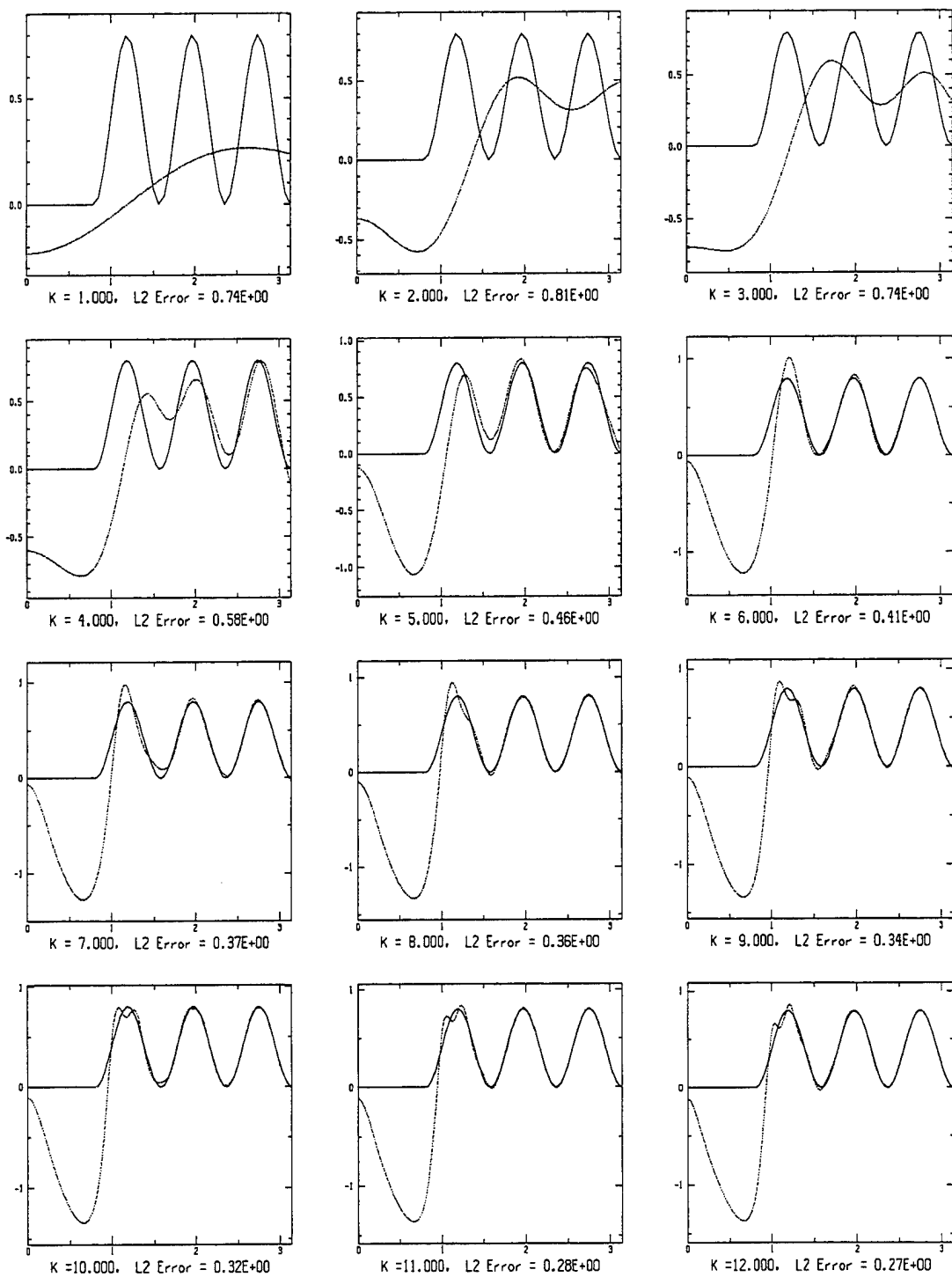Figure 17: Plots of Error Distributions at 9 Frequencies, Example 4.

Figure 18: Reconstructed vs Exact q_5 at 12 Frequencies, Example 5.